UNIVERSIDADE FEDERAL DE MINAS GERAIS
Escola de Engenharia
Programa de Pós-Graduação em Engenharia Metalúrgica, Materiais e de Minas

Paula Campos de Oliveira

Microstructural and mechanical characterization of a Mg-1wt%Mn-1wt%Nd alloy processed by high-pressure torsion

Belo Horizonte
2020

Paula Campos de Oliveira

Microstructural and mechanical characterization of a Mg-1wt%Mn-1wt%Nd alloy processed by high-pressure torsion

Versão final

Dissertação apresentada ao Programa de Pós-Graduação em Engenharia Metalúrgica, Materiais e de Minas da Escola de Engenharia da Universidade Federal de Minas Gerais, como requisito parcial para obtenção do Grau de Mestre em Engenharia Metalúrgica, Materiais e de Minas

Área de Concentração: Metalurgia Física
Orientadora: Profª. Dr.-Ing. Augusta Cerceau Isaac Neta
Coorientador: Prof. Dr. Roberto Braga Figueiredo

Belo Horizonte
2020

Oliveira, Paula Campos de.
O48m Microstructural and mechanical characterization of a Mg-1wt%Mn-1t%Nd alloy processed by high-pressure torsion [recurso eletrônico] / Paula Campos de Oliveira. – 2020.
1 recurso online (93 f.: il., color.): pdf.

Orientadora: Augusta Cerceau Isaac Neta.
Coorientador: Roberto Braga Figueiredo.

Dissertação (mestrado) - Universidade Federal de Minas Gerais, Escola de Engenharia.

Bibliografia: f. 53-65.
Exigências do sistema: Adobe Acrobat Reader.

1. Engenharia Metalúrgica - Teses. 2. Deformações e tensões – Teses. 3. Magnésio – Teses. 4. Metalurgia física – Teses. I. Isaac Neta, Augusta Cerceau.II. Figueiredo, Roberto Braga. III. Universidade Federal de Minas Gerais. Escola de Engenharia. IV. Título.

CDU: 669(043)

Ficha catalográfica elaborada pela Bibliotecária Letícia Alves Vieira - CRB-6/2337
Biblioteca Prof. Mário Werneck - Escola de Engenharia da UFMG

UNIVERSIDADE FEDERAL DE MINAS GERAIS
ESCOLA DE ENGENHARIA
Programa de Pós-Graduação em Engenharia Metalúrgica, Materiais e de Minas

Dissertação intitulada **"Microstructural and Mechanical Characterization of a Mg-1wt.%Mn-1wt.%Nd Alloy Processed by High-pressure Torsion "**, área de concentração: Metalurgia Física, apresentada pela candidata **Paula Campos de Oliveira**, para obtenção do grau de Mestre em Engenharia Metalúrgica, Materiais e de Minas, aprovada pela comissão examinadora constituída pelos seguintes membros:

Profª Augusta Cerceau Isaac Neta
Orientadora - Drª (UFMG)

Prof. Roberto Braga Figueiredo
Coorientador - Dr. (UFMG)

Prof. Pedro Henrique Rodrigues Pereira
Dr. (UFMG)

Prof. Luciano Andrey Montoro
Dr. (UFMG)

Prof. Rodrigo Lambert Oréfice
Coordenador do Programa de Pós-Graduação em Engenharia Metalúrgica, Materiais e de Minas/UFMG

Belo Horizonte, 28 de setembro de 2020

RESUMO

O magnésio é o metal estrutural mais leve, apresentando uma alta resistência específica e oferecendo um considerável potencial para aplicações automotivas e aeroespaciais. No entanto, o seu uso permanece restrito devido a sua baixa formabilidade à temperatura ambiente e a sua baixa resistência mecânica. Para melhorar as propriedades do Mg, algumas das alternativas viáveis são adicionar elementos terras-raras às suas ligas e submeter o material à deformação plástica severa. O presente trabalho investiga a evolução microestrutural e mecânica da liga Mg-1%Mn-1%Nd em peso processada por torção sob alta pressão, e a microestrutura foi caracterizada por difração de raios X, microscopia eletrônica de varredura e de transmissão. A segregação dos elementos de liga foi avaliada com imagens de campo escuro de alto ângulo, e é tipicamente relacionada a uma maior dureza e estabilidade térmica, o que aumenta o interesse em entender sua formação. Os resultados mostram que o Nd segrega rapidamente para os contornos de grão nos estágios iniciais de deformação, enquanto o Mn, que estava disperso em pequenas partículas no material inicial, sofre uma fragmentação lenta, formando nanopartículas distribuídas por toda a microestrutura e segregando para os contornos de uma maneira distintamente mais lenta do que os átomos de Nd. A evolução da microdureza mostra um rápido aumento da resistência mecânica para níveis baixos de deformação, até a sua saturação. Sugere-se que o Mn desempenhe um papel com pouca relevância na contribuição para o aumento de resistência dessa liga, pois o lento desenvolvimento de nano-aglomerados e segregações desse elemento não afeta de forma relevante a dureza.

Palavras-chave: liga de magnésio; deformação plástica severa, torção sob alta pressão; segregação.

ABSTRACT

Magnesium is the lightest structural metal with a high strength-to-mass ratio, offering considerable potential for automotive and aerospace applications. However, its use remains restricted due to its poor formability at room temperature and low strength. To improve the properties of Mg, some of the viable alternatives are alloying with rare-earth elements and subjecting the material to severe plastic deformation. The present work investigated the microstructural and mechanical evolution of a Mg-1wt% Mn-1wt%Nd processed by high-pressure torsion, and its microstructure was characterized by X-ray diffraction, scanning, and transmission electron microscopy. The segregation of alloying elements was observed with high-angular annular dark-field images, and it is typically related to higher hardness and thermal stability, enhancing the interest in understanding their formation. The results show that Nd readily segregates to grain boundaries in early stages of deformation, while Mn, which was dispersed as small particles in the starting material, undergoes slow fragmentation forming nanoparticles distributed throughout the microstructure, and segregates to boundaries in a distinctly more sluggish manner than Nd atoms. The evolution of microhardness shows a rapid increase in strength at low imposed strains until reaching saturation. It is suggested that Mn plays only a minor role in the contribution to the strength of this alloy because the slow development of nanoclusters and segregations of this element does not relevantly affect the hardness.

Keywords: magnesium alloy; severe plastic deformation; high-pressure torsion; segregation.

LIST OF FIGURES

LIST OF ABBREVIATIONS

ADF	annular dark-field
APT	atom probe tomography
Bcc	body-centered cubic
BF	bright-field
EBSD	electron backscattered diffraction
ECAP	equal-channel angular pressing
EDS	energy dispersive X-ray spectrometry
Fcc	face-centered cubic
FFT	fast Fourier transform
FIB	focused ion beam
GB	grain boundary
HAADF	high-angle annular dark-field
HAGB	high-angle grain boundary
Hcp	hexagonal close-packed
HPT	high-pressure torsion
HRTEM	high-resolution transmission electron microscopy
LAGB	low-angle grain boundary
RE	rare-earth
SAD	selected area diffraction
SEM	scanning electron microscopy
SPD	severe plastic deformation
STEM	scanning transmission electron microscopy
TEM	transmission electron microscopy

UFG	ultrafine-grained
XRD	X-ray diffraction

LIST OF SYMBOLS

Mg	Magnesium
Mn	Manganese
Nd	Neodymium
MN11	Mg-1wt%Mn-1wt%Nd alloy
m	Meter
N	Number of turns during the HPT process
g	Gram
cm	Centimeter
Al	Aluminum
Fe	Iron
σ_y	Yield stress
σ_0	Friction stress when dislocations glide on the slip plane
k	Stress concentration factor
d	Average grain size
nm	Nanometer
d*	Critical grain size
σ_c	Critical stress
G	Gadolinium
Y	Yttrium
Dy	Dysprosium
Zn	Zinc
Zr	Zirconium
J_v	Vacancy flux

Ce	Cerium
M1	Mg-1wt%Mn alloy
°C	Degree Celsius
Si	Silicium
b	Burgers vector
r_p	Particle radius
AZ31	Mg–3wt%Al–1wt%Zn alloy
AZ80	Mg-8wt%Al-0.5wt%Zn alloy
AZ91	Mg–9wt%Al– 1wt%Zn alloy
P	Pressure
GPa	Gigapascal
ε_{eq}	Equivalent von Mises strain
r	Radius of the disk processed by HPT
h	Thickness of the disk processed by HPT
AZ61	Mg–6wt%Al–1wt%Zn alloy
Cu	Copper
HV	Vickers hardness number
mm	Milimeter
EZ33A	Mg-2.5wt%Zn-0.4wt.%Zr-3wt.%RE alloy
MPa	Megapascal
K	Kelvin
ω	Angular frequency
rpm	Revolutions per minute
$\dot{\varepsilon}$	Strain rate

s	Second of time
Z	Atomic number
μm	Micrometer
kV	Kilovolt
gf	Gram-force
Cr	Chromium

TABLE OF CONTENTS

1INTRODUCTION

The increasing demand for energy is becoming a critical issue due to its environmental impact and the scarcity of resources. To overcome this challenge, the development of lightweight materials is a core target for the automotive and aerospace industries. In this context, magnesium is of great interest since it is the lightest structural metal while having a high strength-to-mass ratio. Besides reducing fuel consumption, Mg is easily recyclable when compared with polymers, and it is also biocompatible, making it attractive for biomedical applications. Nevertheless, despite being a compelling material from a sustainability standpoint, broader use of Mg is restricted because of its low formability at room temperature and poor mechanical properties in comparison to conventional alloys.

The difficulty in deforming Mg alloys is linked to their hexagonal close-packed structure, which has fewer slip systems at lower temperatures in comparison with face-centered cubic and body-centered cubic metals. To overcome its poor mechanical properties, alloying Mg with rare-earth (RE) elements has been leading to great results because there is an improvement in the ductility with the increase of cross-slip and multiplication rate. Moreover, the strength of Mg-RE alloys can be enhanced by age hardening, a heat treatment that produces fine precipitates of a second phase within the alloy, impeding the movement of dislocations. Despite this potential to raise strength via age hardening, multiple studies have reported lackluster results, especially when compared with aluminum alloys. Attempts to enhance the age-hardening response of Mg alloys demands an in-depth comprehension of the precipitates, such as their morphology, size, volume fraction, and the nature of the interface between the particles and the matrix.

The Mg-1wt%Mn-1wt%Nd alloy (MN11) has been showing satisfactory results, such as inducing weaker textures, which leads to an increase in ductility in a particular loading direction, and reducing the tension–compression yield asymmetry. Among the RE elements, it appears that Nd is the most effective to weaken the texture. Manganese is often added to Mg alloys because it increases corrosion resistance and improves the creep behavior. The alloying elements interact with the dislocations in different ways, and Nd forms a variety of intermetallic compounds with Mg, while Mn does not form such

compounds. This contrasting behavior of Nd and Mn makes MN11 an interesting alloy to evaluate how each element contributes to the strengthening mechanisms.

The strength of Mg-RE alloys can be further enhanced with severe plastic deformation (SPD), which produces an extraordinary grain refinement. High-pressure torsion (HPT) has been the most successful SPD technique to produce ultrafine-grained Mg alloy since it consists of the application of a hydrostatic pressure at the same time as a large torsional strain, preventing fracture and cracking. Notoriously, HPT induces the formation of supersaturated solid solutions and segregations of alloying elements to grain boundaries, but the mechanisms responsible for these phenomena are not yet clarified.

With the objective of having a better understanding of the strengthening mechanisms of Mg-RE alloys, this study aimed to examine the microstructure and mechanical properties of an extruded MN11 alloy processed by HPT for different strain levels. To attain this goal, I used scanning electron microscopy (SEM) alongside energy dispersive X-ray spectrometry (EDS), and X-ray diffraction (XRD) to determine the existent phases. In particular, I examined the distribution of phases and the segregation of elements to grain boundaries using high-angle annular dark-field scanning transmission electron microscopy (HAADF-STEM), an imaging technique with atomic resolution. To assess the influence of HPT on the mechanical properties, I carried out microhardness tests.

In this thesis, I first present a bibliographic review with important scientific concepts to comprehend this work, in addition to the latest and most relevant research carried out in the area. Then, I show the results and discussion through the article "Development of segregations in a Mg-Mn-Nd alloy during HPT processing", which was submitted to Materials Science and Engineering: A.

INTRODUÇÃO

A crescente demanda por energia está se tornando um problema crítico devido ao seu impacto ambiental e à escassez de recursos. Para superar esse desafio, o desenvolvimento de materiais leves é um objetivo central das indústrias automotiva e aeroespacial. Nesse contexto, o magnésio é de grande interesse, pois é o metal estrutural mais leve, ao mesmo tempo que possui uma alta força específica. Além de reduzir o consumo de combustível, o Mg é facilmente reciclável quando comparado aos polímeros, além de ser biocompatível, o que o torna interessante para aplicações biomédicas. No entanto, apesar de ser um material atrativo do ponto de vista da sustentabilidade, um uso mais amplo de Mg é restrito por causa de sua baixa formabilidade à temperatura ambiente e de suas propriedades mecânicas pobres em comparação com ligas convencionais.

A dificuldade em deformar ligas de Mg está ligada a sua estrutura hexagonal compactada, que tem menos sistemas de escorregamento em temperaturas mais baixas em comparação com metais cúbicos de face centrada e cúbicos de corpo centrado. Para superar suas fracas propriedades mecânicas, a adição de elementos terras-raras (*RE*) às ligas de Mg tem levado a grandes resultados, pois há um melhora da ductilidade com o aumento do escorregamento cruzado e da taxa de multiplicação. Ademais, a resistência mecânica das ligas de Mg-RE pode ser melhorada mediante o envelhecimento, um tratamento térmico que produz precipitados finos de uma segunda fase dentro da liga, impedindo o movimento de deslocações. Apesar desse potencial para o aumento da resistência por meio do endurecimento por precipitação, vários estudos apresentaram resultados decepcionantes, especialmente quando comparados com ligas de alumínio. As tentativas de melhorar a resposta ao envelhecimento das ligas de Mg exigem uma compreensão profunda dos precipitados formados, como por exemplo das suas morfologias, dos seus tamanhos, da sua fração de volume e da natureza da interface entre as partículas e a matriz.

A liga Mg-1%Mn-1%Nd em peso (MN11) vem apresentando resultados satisfatórios, tais como a indução de texturas mais fracas, o que leva ao aumento da dutilidade, e a diminuição da assimetria tensão-compressão do escoamento. Entre os elementos terras-raras, parece que o Nd é o mais eficaz para enfraquecer a textura. O manganês é

frequentemente adicionado às ligas de Mg pois aumenta a resistência à corrosão e melhora o comportamento em fluência. Os elementos de liga interagem com as deslocações de diferentes maneiras, e o Nd forma uma variedade de compostos intermetálicos com o Mg, enquanto o Mn não forma compostos do tipo. Esse comportamento contrastante entre Nd e Mn torna a liga MN11 interessante para avaliar como cada elemento contribui para os mecanismos de endurecimento.

A resistência das ligas de Mg-*RE* pode ser aumentada mais ainda com deformação plástica severa (*SPD*), que produz um extraordinário refino de grão. A torção sob alta pressão (*HPT*) tem sido a técnica de *SPD* de maior sucesso para a produção de ligas de Mg de granulação ultrafina, pois consiste na aplicação de uma pressão hidrostática ao mesmo tempo que uma grande tensão de torção, evitando fraturas e trincas. Notoriamente, o *HPT* induz a formação de soluções sólidas supersaturadas e segregações de elementos de liga para contornos dos grãos, mas os mecanismos responsáveis por esses fenômenos ainda não foram esclarecidos.

Com o objetivo de ter uma melhor compreensão dos mecanismos de endurecimento das ligas de Mg-*RE*, este estudo teve como objetivo examinar a microestrutura e as propriedades mecânicas de uma liga MN11 extrudada e processada por *HPT* para diferentes níveis de deformação. Para atingir esse propósito, usei microscopia eletrônica de varredura (*SEM*) juntamente com espectroscopia de raios X por dispersão em energia (*EDS*) e difração de raios X (*XRD*) para determinar as fases existentes. Em particular, examinei a distribuição de fases e a segregação de elementos para contornos de grão usando imagens de campo escuro de alto ângulo em microscópio eletrônico de varredura (*HAADF-STEM*), uma técnica de imagem com resolução atômica. Para avaliar a influência do *HPT* nas propriedades mecânicas, realizei testes de microdureza.

Nesta dissertação, eu inicialmente apresento uma revisão bibliográfica com conceitos científicos importantes para a compreensão deste trabalho, além das pesquisas mais recentes e relevantes realizadas na área. Em seguida, eu mostro os resultados e a discussão através do artigo "*Development of segregations in a Mg-Mn-Nd alloy during HPT processing*", que foi submetido à *Materials Science and Engineering: A*.

2 OBJECTIVES

2.1 General objective

This study aimed to investigate the microstructural evolution in a MN11 alloy following processing by HPT to different strain levels.

2.2 Specific objectives

- To analyze the chemical mixing of the alloy constituents from the micrometer to the atomic scale during the HPT processing for different number of turns (N = 0, ¼, 1, 2 and 5) by means of scanning transmission electron microscopy, scanning electron microscopy and X-ray diffraction;
- To evaluate the mechanical properties of HPT-processed MN11 alloy for different numbers of turns by microhardness measurements;
- To correlate the microstructural characteristics of the HPT-processed samples with the mechanical properties.

3 SCIENTIFIC BACKGROUND

This chapter provides the importance of studying magnesium alloys, especially those which contain rare-earth elements. The progress in the study of these alloys is addressed, as well as the main research perspectives in the area.

The HPT process is discussed, along with its influence on mechanical properties. Methods of microscopy used in this investigation, such as HAADF-STEM, are also studied.

3.1 Magnesium alloys

Over the decade, magnesium alloys have been attracting attention from the industry and scientists alike, since Mg is an interesting material from an ecological point of view. It is the lightest structural metal, with a density of 1.74 g/cm^3, about 2/3 of Al density and 1/4 that of Fe, and has a high strength-to-mass ratio. Weight reduction is crucial in energy efficiency - a 10% reduction in vehicle weight is expected to decrease fuel consumption by 6-7%[1]. In addition to being lightweight, its availability and recyclability make Mg compelling for a sustainable development. Despite all these advantages, the automotive and aerospace industries are still resistant to a wider application of Mg alloys due to their low ductility and formability at room temperature. These poor mechanical properties are linked to the deformation mechanisms of Mg, which are more complex than those of common engineering materials.

3.1.1 *Deformation mechanisms of Mg and Mg-RE alloys*

Differently from other structural metals, such as Fe and Al, Mg does not have a cubic symmetric structure like body-centered cubic (bcc) and face-centered cubic (fcc), but a hexagonal close-packed (hcp) one, linked to the poor formability presented by Mg. At low temperatures, this structure presents only two independent easy slip systems, involving $\frac{1}{3} < 11\bar{2}0 >$ basal slip with a < **a** > type Burgers vector, as seen in Figure 3.1[2,3]. The most common slip systems are $(0001) < 11\bar{2}0 >$ basal and $\{10\bar{1}0\} < 11\bar{2}0 >$ prismatic, both with a < **a** > type Burgers vector, and they offer just four independent slip

modes between them. Therefore, in those conditions, the hcp crystal fails to satisfy the von Mises yield criterion, which states that five independent slip systems are required to enable a homogeneous plastic deformation. Even if < **a** > type basal and prismatic slip systems cross-slip, only four independent modes are possible. However, the activation of a slip system with non-basal < **c** + **a** > Burgers vectors provides the obtainment of the required five independent modes[2].

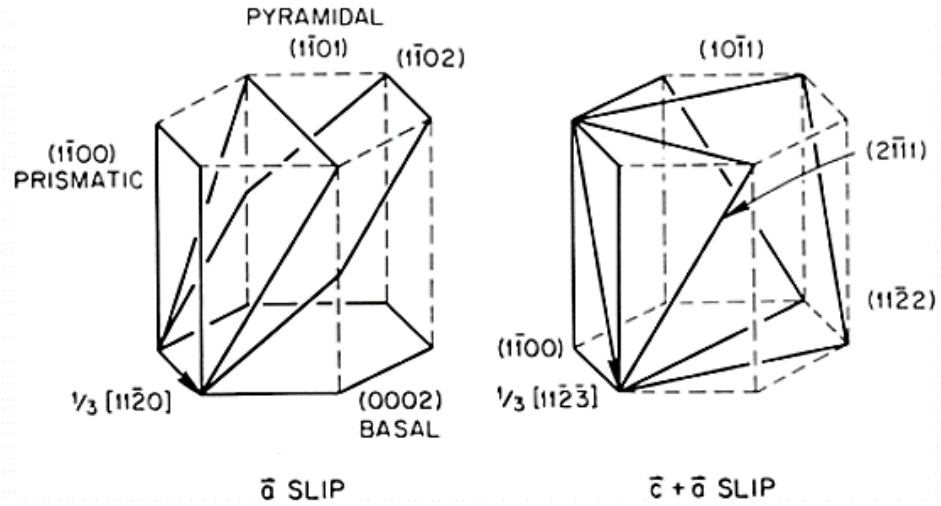

Figure 3.1 – Basal, prismatic, and pyramidal slip systems with < a > Burgers vector, and four possible pyramidal slip planes with < c + a > Burgers vector.
[YOO, 1981[3]]

For many years, the deformation mechanisms of magnesium were not understood. Recently, the origins of the low ductility in magnesium were clarified in studies made by Wu and Curtin (2015, 2018)[4,5]. In the first study, it was shown through long-time molecular dynamics simulations that the < **c** + **a** > dislocations, essential to the general plasticity, are metastable on easy-glide pyramidal II planes. These dislocations transition into an immobile structure at room temperature due to a decrease in their energy. The plastic slip in the c-axis direction is therefore restricted, resulting in a low ductility. It is possible to prevent those transitions by additions of solute – some other researchers[6–8] indicate that alloying Mg with RE elements increases its ductility because it stabilizes the easy-glide < **c** + **a** > dislocation. In the more recent study, they explain that the optimization of the alloy composition allows the increasing of cross-slip and multiplication rates of < **c** + **a** > dislocations, favoring high ductility[5].

Another important deformation mechanism of Mg is twinning, especially at low temperatures and high strain rates[9]. Kocks and Westlake (1967)[10] argued that twinning would allow polycrystalline hexagonal materials to undergo general plastic deformation without the need for five independent slip systems. Inelastic strains cause internal stresses at grain boundaries, and local deformation by twinning may relieve them. This was proved by Hutchinson (1977)[11], who has shown a polycrystalline material that deformed uniformly with only four independent slip systems and without the < **c** + **a** > pyramidal slip. Some twin modes have been correlated to a low ductility, and several studies aimed to reduce their development with grain size reduction or alloying[12–15]. Given the mentioned deformation mechanisms, it is essential to understand how different elements affect the mechanical properties of Mg alloys to develop high-performance materials.

3.1.2 *Strengthening mechanisms*

The main premise of strengthening a material is creating obstacles to dislocations, since their movement in large-scale induces macroscopic plastic deformation. To enhance the strength of Mg alloys, some of the principal mechanisms are strain hardening, grain boundary strengthening, solid solution strengthening, and precipitation hardening.

Strain hardening, also known as work hardening or cold working, is the strengthening of a material by plastic deformation, exerting a great influence on the mechanical properties of Mg alloys according to various studies[16–19]. During plastic deformation, dislocations multiply and new ones are created, and thus the number of dislocations dramatically increases. Consequently, the dislocations entangle with one another, and the motion of dislocations becomes more difficult[20].

Due to the strong plastic anisotropy and the more complex nature of Mg deformation mechanisms, explained in the previous chapter, strain hardening in Mg alloys is not yet fully understood. Numerous studies have been conducted to clarify how parameters such as grain size, twinning, texture, temperature, second phase particles, and strain rate affect strain hardening[21–23]. For instance, Imandoust, Barret, and El Kadiri (2018)[23] have studied the effect of RE elements addition on the strain hardening related to $\{10\bar{1}2\}$

twinning. As mentioned in the last chapter, RE elements generally increase the ductility of Mg alloys since they prevent the transition of the < c + a > dislocations to immobile structures, which are deleterious for plastic deformation. However, in this study, they have demonstrated that Gd and Ce additions in Mg after extrusion enhance the flow stress. They associated this phenomenon to the fact that the entanglement of dislocations, known as forest hardening, overshadowed the RE-induced < c + a > softening. The increase in work hardening is attributed to the influence of solute drag on dislocation dynamics and preferential RE segregation to grain boundaries[24–26].

The grain boundary strengthening is based on the reduction of grain size. To clarify this mechanism, Figure 3.2[27] shows the motion of a dislocation as it encounters a grain boundary. For a dislocation to move into another grain, it must change its direction, and rarely the grain B has a similar slip plane to that of the dislocation moving in crystal A. Thus, dislocations pile up at high-angle grain boundaries due to the crystallographic misorientation between the grains, requiring a large amount of energy for a dislocation to overcome. Since grain boundaries act as barriers to the movement of dislocations, the smaller the grain size, the harder and stronger is the material, because fine-grained materials have a greater grain boundary area, which limits the mean free path of the dislocations[20]. The piled-up dislocations introduce stress concentrations ahead of their slip planes, being a source of new dislocations in adjacent grains after reaching a critical value, and thus enabling the deformation of the grain, as illustrated in Figure 3.3[20,28–30].

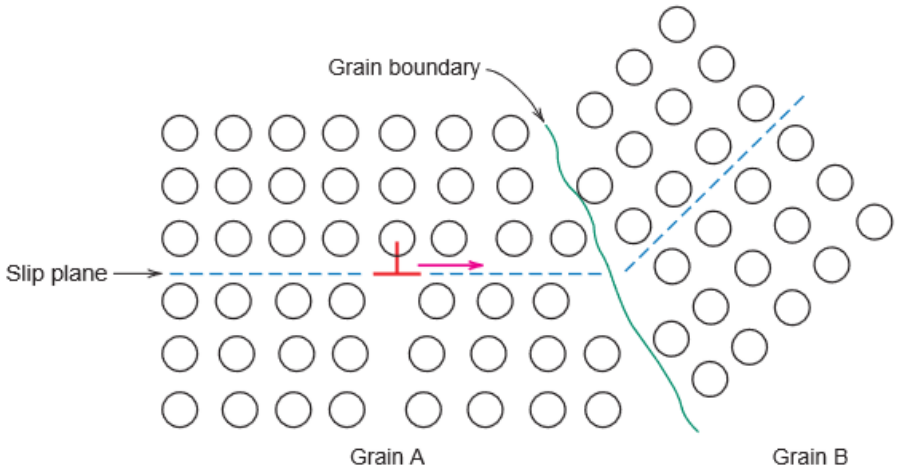

Figure 3.2 – Dislocation moving as it encounters a grain boundary, depicting how the grain boundary acts as an obstacle to continued slip.

[VAN VLACK, 1973[27]]

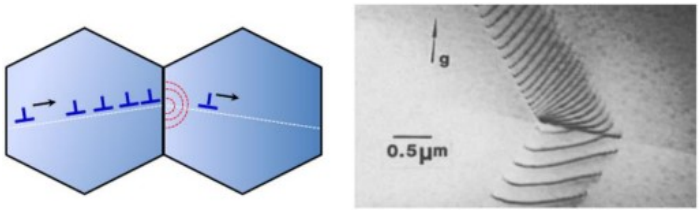

Figure 3.3 – Diagrams showing slip propagation from one grain to the neighboring grain, and TEM image showing dislocation transfer behavior.
[Adapted from YU et al., 2018[28]]

For many materials, the effect of grain size on the strength, represented by the yield stress σ_y, is expressed by the Hall-Petch relationship, given by the equation 3.1[31]:

$$\boldsymbol{\sigma_y = \sigma_0 + kd^{-\frac{1}{2}}} \tag{3.1}$$

where σ_y is the yield stress, d is the average grain size, and k and σ_0 are material constants, known as stress concentration factor and friction stress when dislocations glide on the slip plane, respectively.

The Hall-Petch relationship was developed based on highly isotropic materials. Even though this equation is also applicable to Mg alloys, the fact that they usually are highly anisotropic and strongly textured makes this relationship more complicated[32,33]. The Hall-Petch parameters, such as *k*, change if texture or loading direction is altered. Yu et al. (2018)[28] have summarized *k* values for different Mg alloys as functions of the processing condition and loading path within a given range of grain size.

When the grain size reduction reaches a critical value, usually from 10 to 30 nm, the Hall-Petch relation is not applicable. In fact, a softening mechanism is observed, which is known as the inverse Hall-Petch effect[34]. Pande and Masumura (1996)[35] were the first to explain this phenomenon in nanocrystalline materials by using a mathematical extrapolation of the conventional lattice dislocation slip model[36], taking into account that small grain sizes prevent a large number of dislocations in a pile-up. In a similar model, Malygin (1995)[37] has suggested that, in nanocrystalline materials, the grain boundaries act as sinks of dislocations. This is contrary to what was proposed by Li (1963)[30], who

considered the boundaries as sources for dislocations. However, these models may not be applicable depending on the grain size because nanocrystalline solids may present reduced density or even absence of lattice dislocations due to the instability of these defects in confined nanophase grains[38–40]. Therefore, another deformation mechanism had to be considered for small grain sizes. Chokshi et al. (1989)[41] were the first to suggest grain-boundary diffusional creep as the main deformation mode in nanocrystalline materials. This form of creep is known as Coble creep[42], and essentially consists in the movement of vacancies along grain boundaries, whereas in the Nabarro–Herring creep[43], the vacancies move through the crystal[9,34]. Several studies[44–46] have reported the importance of Coble creep in fine-grained Mg alloys. Nevertheless, this Coble creep argument does not explain the behavior in materials with grain size in the intermediate range (20 ± 200 nm). For that, Masumura, Hazzledine, and Pande (1998)[47] established a transition regime between the Hall–Petch and Coble creep-like behavior. In this model, they assumed that polycrystals with a relatively large average grain size obey the classical Hall–Petch relation expressed in Eq. 3.1, and for very small grain sizes, they concluded that Coble creep is active, as illustrated in Figure 3.4[47,48]. Recently, Naik and Walley (2020)[49] explained the inverse Hall-Petch effect through the transition from dislocation-based plasticity to a grain boundary sliding mechanism that may occur in nanosized grains. However, the subject is still controversial because the effect could result from processing artifacts or stress-induced grain growth during testing[49,50].

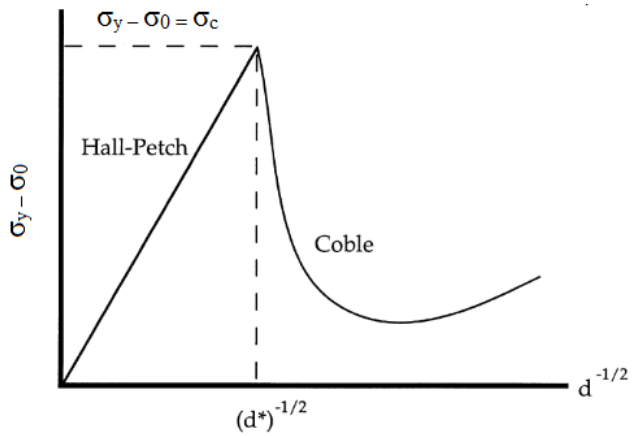

Figure 3.4 – Illustration of the transition regime between Hall-Petch and Coble creep according to the grain size *d*. The dashed line denotes the critical *d** where transition occurs, and σ_c is the respective critical strain.

[Adapted from MASUMURA, HAZZLEDINE & PANDE, 1998[47]]

Solid solution hardening is another mechanism to strengthen and harden Mg alloys, and it consists of alloying the metal with impurity atoms, imposing lattice strains on the adjacent host atoms. Solute atoms in Mg alloys change the lattice constants and modify the binding forces, forming a substitutional solid solution, when large enough to replace the solvent atoms, or an interstitial solid solution, when small enough to fit the interstitial sites between the solvent atoms. The dislocations interact with the lattice strain field, and therefore the resistance to slip is increased, as illustrated in Figure 3.5. The solute atoms segregate around dislocations at certain positions to reduce the overall strain energy, canceling some of the strain in the lattice[20].

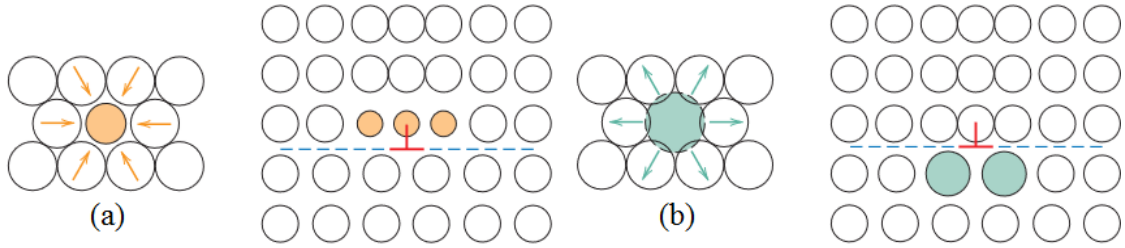

Figure 3.5 - Representation of (a) tensile lattice strains imposed on host atoms by a smaller substitutional impurity atom and of (b) compressive strains imposed by a larger substitutional impurity atom, and the possible locations of the impurity atoms relative to an edge dislocation such that there is partial cancellation of impurity–dislocation lattice strains.
[Adapted from CALLISTER, 2018[20]]

A higher solubility is achieved when solvent and solute atoms have similar atomic sizes. According to the Hume-Rothery rules, their size misfit must be lower than 15% to form a solid solution[20]. Nevertheless, several studies[51–53] have shown that RE elements such as Gd, Y, and Dy contribute more to the strengthening than solutes like Zn, Al, Zr, and Zn, even though they have a larger atomic size difference regarding Mg. Researchers[51,54,55] have found that the other factor affecting the solid solution hardening is related to the covalent bonds formed between RE and Mg atoms, which are stronger than the bonds formed with the other previously mentioned elements. Therefore, they proposed that the valence effect is possibly responsible for the enhanced solid solution strengthening of RE in Mg since the effect of solute additions is not only due to the atomic size misfits but also because of the electron state between the atoms.

Precipitation hardening, also known as age hardening, is a heat treatment carried out to enhance the material strength through the production of dispersed fine particles of a second phase, hindering the movement of dislocations. The process is represented in Figure 3.6 and consists firstly on a solution treatment, in which the material is heated above the solvus temperature and held for some time to fully dissolve the coarse second-phase precipitates. The material is then quenched to obtain a supersaturated solid solution. Subsequently, the aging treatment occurs through heating the alloy for a certain time and at a temperature below the solvus line, obtaining a controlled decomposition of the supersaturated solid solution. Finally, a fine distribution of precipitates in the magnesium matrix is achieved[20].

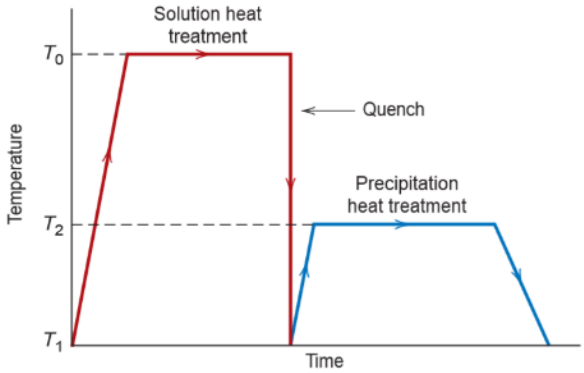

Figure 3.6 – Schematic temperature-versus-time plot showing the stages of the process of precipitation hardening.
[CALLISTER, 2018[20]]

Despite the potential to increase strength via age hardening, multiple studies have reported a lackluster improvement of mechanical properties, especially when compared to Al alloys[56–60]. In the past century, some precipitate phases and precipitation sequences could not be clearly established because of the limitations and low resolution of transmission electron microscopy (TEM) characterization. Nevertheless, with the advent of HAADF-STEM in recent years, the identification of precipitates is greatly facilitated, attracting the attention of researchers who have been eager to unravel this puzzle. HAADF-STEM is an imaging technique with atomic resolution and may be used to determine the structure, morphology, and orientation of precipitates. Knowing the crystallography of precipitate phases may provide comprehensive information on the strengthening mechanisms of Mg. More importantly, such understanding leads to the design of optimized alloys with better mechanical and chemical properties[56].

3.1.3 *Mg-Mn-Nd alloy*

As discussed previously, alloying Mg with RE elements may provide diverse benefits, such as the increase of ductility, formability, and strength. Besides these advantages, the alloy under study presents other interesting aspects. Bohlen et al. (2010) [61] investigated the influence of different RE elements on the microstructure and texture of Mg-Mn samples formed during indirect extrusion and the resulting mechanical properties. The study found that Nd is a much stronger texture modifier than Ce or Y in Mg-Mn alloys. The weaker texture caused by Nd leads to an increase in ductility and a decrease in the asymmetric yield behavior, but it also contributes to a lower yield and ultimate stresses. These mechanical properties are represented in Figure 3.7, comparing the behavior in tension and compression of alloys MN11 and M1 (Mg-1wt%Mn)[62].

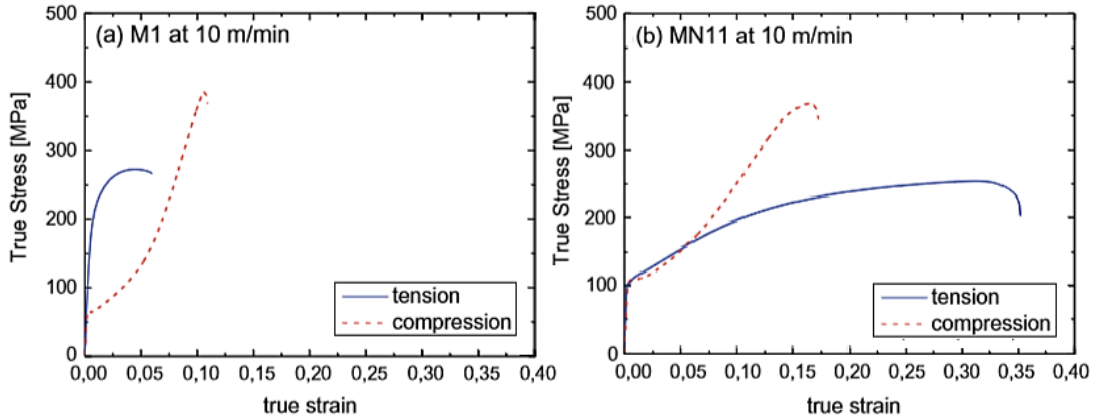

Figure 3.7 – True stress vs. strain curves in tension and compression of (a) M1 alloy; (b) MN11 alloy after indirect extrusion at 10m/min.
[BOHLEN, 2009[62]]

In the literature, there are few reports of ternary diagrams of Mg-Mn-Nd alloys. Mostafa et al. (2012)[63] has conducted an experimental investigation combined with a thermodynamic simulation of eight different compositions of Mg-Mn-Nd alloys, identified in Figure 3.8. After heat treatment at 450 °C, XRD results were used to identify the existent phases, such as Mn and intermetallic phases Mg_3Nd and $Mg_{12}Nd$. The MN11 alloy has a low concentration of Mn and Nd, and therefore it is expected to have Mn precipitates and Mg-Nd intermetallics. It is also possible to have Mn-Nd intermetallics, but it is improbable due to their small quantities.

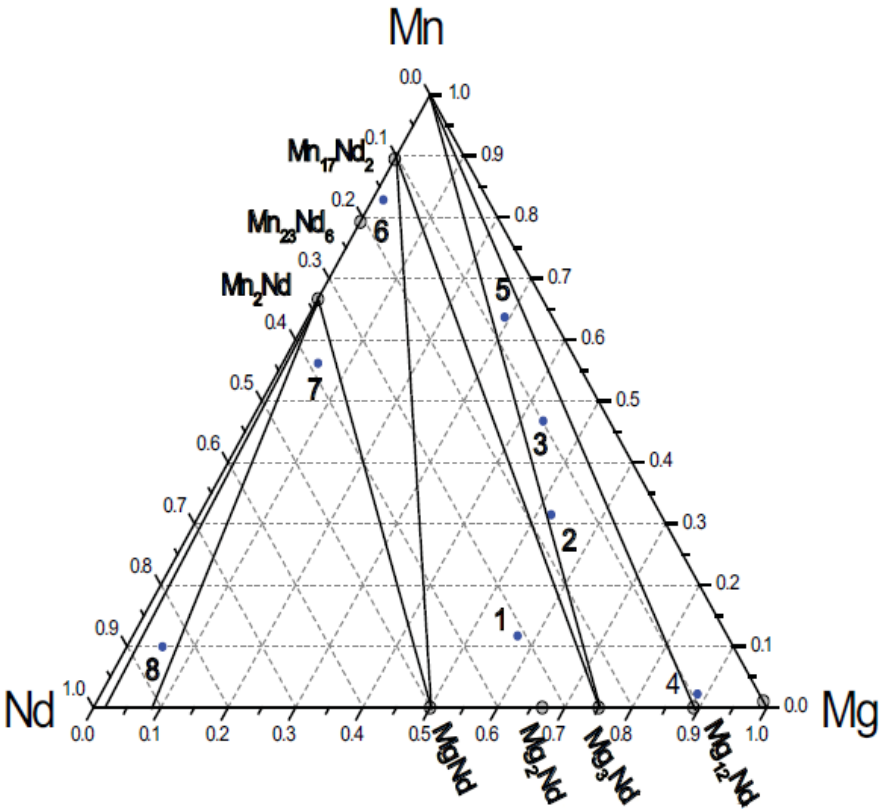

Figure 3.8 – Ternary diagram of Mg-Mn-Nd at 450 °C.
[MOSTAFA, 2012[63]]

Figure 3.9 shows the phase diagram of the Mg-Nd binary system[64]. It is possible to perceive a sharp decrease in the solubility of the Nd in Mg with declining temperature, which is a necessary criterion for the precipitation hardening. It is also possible to notice the existence of three thermodynamically stable intermetallic phases at room temperature: MgNd, Mg_3Nd, and $Mg_{41}Nd_5$. At the temperature of 675 °C, the Mg_2Nd intermetallic compound is also present.

According to the binary diagram Mg-Nd, there are a variety of intermetallic compounds that can be obtained. However, predicting which phases will indeed be formed is a complicated task. The competition between the driving force to precipitate a second phase and the energy barrier that must be overcome to create a new precipitate structure generally leads to a sequence of metastable precipitation. The reason why it is so difficult to predict this precipitation sequence is that the structures involved in the initial stages of the decomposition are not thermodynamically stable. Therefore, the sequences of metastability must be determined empirically[65].

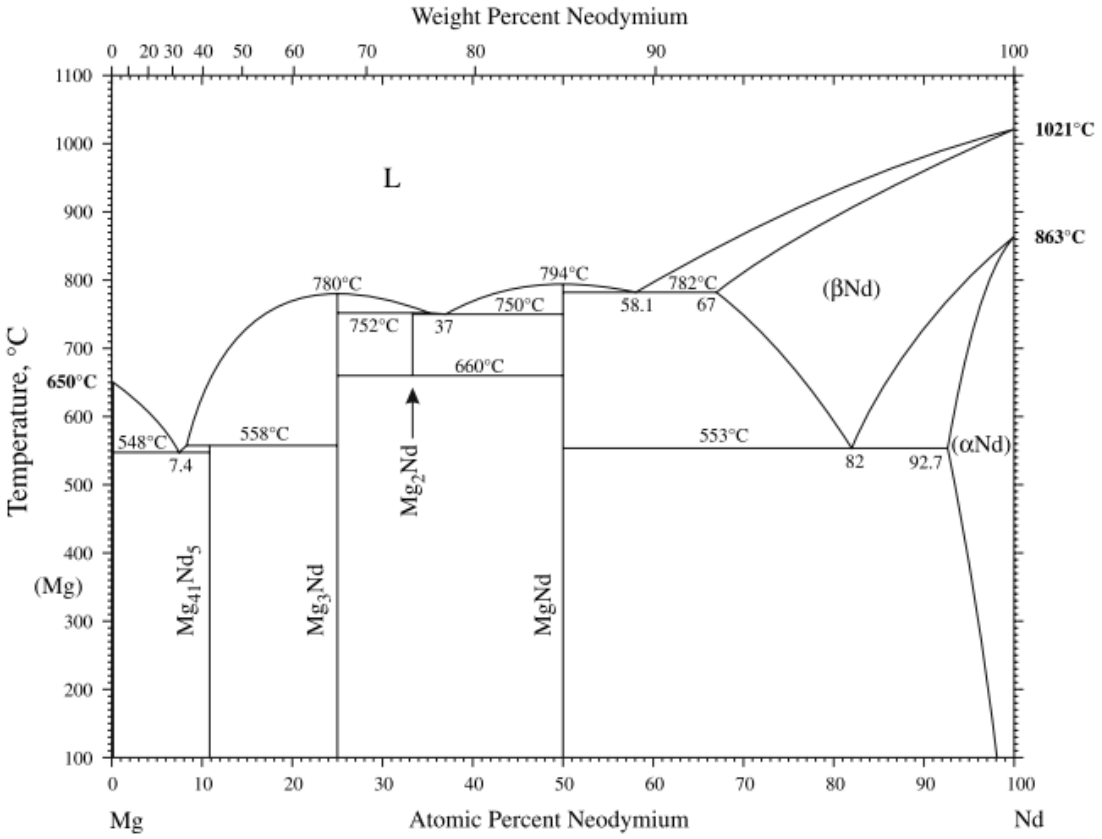

Figure 3.9 – Mg-Nd phase diagram.
[OKAMOTO, 2017[64]]

Various studies[57,60,66,67] focused on determining the sequence of precipitation and the morphologies and compositions of the metastable phases in the early stage of Mg-Nd alloy aging, with the use of modern imaging techniques such as HAADF-STEM and atom probe tomography (APT). However, those characteristics of precipitates are still a controversial issue[56,57,68].

Another important diagram to be considered in this work is the binary phase diagram of Mg-Mn, illustrated in Figure 3.10[69]. Manganese is an interesting addition to Mg alloys because it increases corrosion resistance, removing deleterious elements like Fe and Si by forming harmless intermetallics[70]. A further advantage of using Mn is the improvement of the creep behavior because of the dynamic precipitation of α-Mn on the basal planes of Mg during creep, which hinders the motion of dislocations[71,72]. From the diagram, it can be seen that Mg and Mn are practically immiscible in the solid phase. Mn has such a low solubility in Mg due to some reasons: it has a large atomic size misfit with

Mg; their crystalline structures are very different (Mg is hcp, Mn is bcc); and the diffusion of Mn atoms into the Mg matrix is slow. Because of it, Mn forms fine and stable precipitates at high temperatures, exerting a strong pinning force on grain boundaries. Therefore, the fine precipitates of Mn inhibit grain boundary migration, contributing to the invariance of the grain size of the alloy upon heat treatment[73–75].

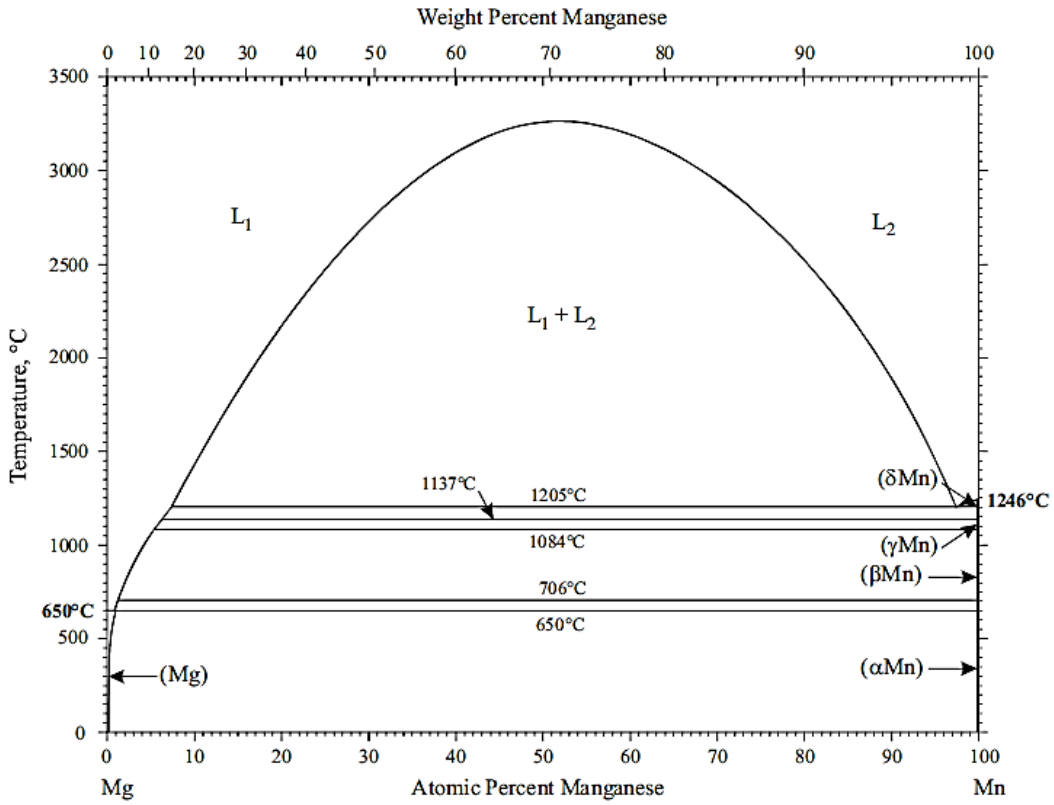

Figure 3.10 – Binary diagram of Mg-Mn
[OKAMOTO, 2015[69]]

Given the precipitates that may be present in the MN11 alloy, it is important to study how they interact with the displacements, to obtain the maximum age hardening. The strengthening caused by a precipitate dispersion essentially depends on the particle size, volume fraction, and morphology, and the nature of the boundary between the particle and the matrix. In essence, there are two mechanisms by which a dislocation moves despite the precipitates: the dislocations either shear the second phase particles or resist cutting for being large or "hard" enough, forcing dislocations to move around the particles to bypass them. There are two methods for this detour to occur: by looping, known as Orowan bowing, or by cross slip, known as Hirsch mechanism[76].

The shearing mechanism, shown in Figure 3.11, mainly occurs when the precipitate is coherent with the matrix, that is, its crystal structure and lattice parameters are closely similar to the ones of the matrix. At the time of shearing, the top part above the slip plane will be displaced by a Burgers vector *b* in relation to the bottom part. This interface formation during the shearing makes it necessary to apply more stress to compensate for the additional energy caused by the increase in surface area. Moreover, other important contributions for the yield stress are the further work required to create an antiphase boundary in the case of precipitates with an ordered lattice, and the stresses arising from the coherency strains around the precipitate that does not exactly match the matrix[77–80].

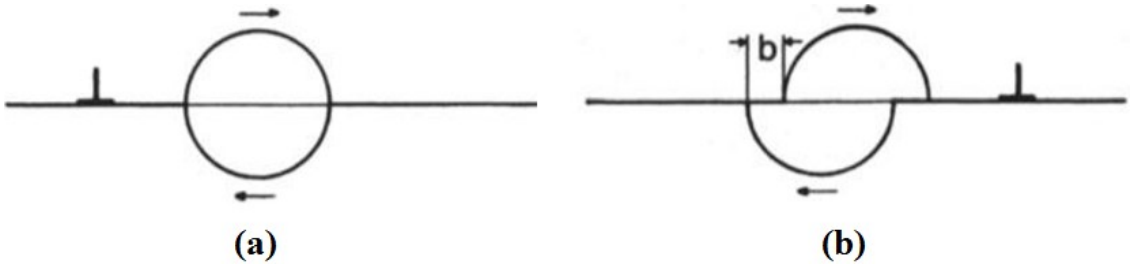

Figure 3.11 - Process of shearing a precipitate through the penetration of an edge dislocation (a) before the dislocation cuts the particle (b) after the shearing.
[Adapted from GOTTSTEIN, 2004[78]]

When the precipitate is incoherent with the matrix, the structures of the two phases are so distinct that the interface is similar to a high-angle grain boundary. Therefore, it is not possible for the dislocations to easily shear the particle, but the precipitate can be bypassed through the Orowan mechanism, as shown in Figure 3.12(a), or through the Hirsch mechanism, as depicted in Figure 3.12(b-d). The Orowan bowing consists of the expansion of dislocations loops around particles until the endings of the created loops annihilate each other, as in a Frank-Read source. This annihilation enables the dislocation to move but leaves a dislocation ring around the particles, which increases resistance to the motion of the next dislocation because of the stress field it generates. The Hirsch mechanism involves the cross slip of screw segments to overcome the particles, leaving a prismatic loop near them[76,78,80,81].

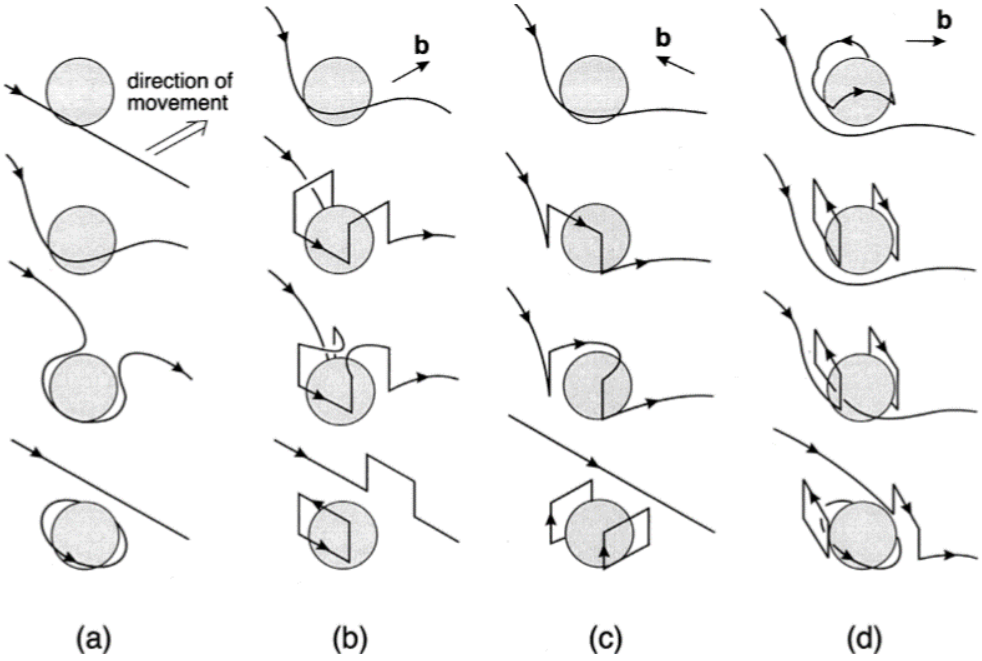

Figure 3.12 – Process of bypassing a precipitate (a) without cross slip, by the Orowan mechanism, (b-d) with cross slip, through the Hirsch mechanism. The Burgers vector is represented by *b*.
[HULL & BACON, 2001[63]]

The transition of the dislocation-particle interaction mechanism from shearing to looping (Orowan) is represented in Figure 3.13. When the particles have a small radius r_p, they are coherent with the matrix and easily sheared by the dislocations, as represented by the small critical resolved shear stress (CRSS). After reaching a critical radius during aging, where the strengthening is maximum, it is easier for the precipitate to create a new incoherent interface than to provide enough elastic strain energy to "match" the adjacent matrix lattices. Therefore, the precipitate is non-deformable, and the dislocation-particle interaction is carried out by the Orowan mechanism. It is interesting to notice that the strengthening during the Orowan regime depends more on the particle radius ($\propto 1/r_p$) than when the interaction was dictated by particle shearing ($\propto r_p^{1/2}$). Thus, when the particle is sheared, the alloy strength varies more with the intrinsic properties of the precipitates than with particle radius, whereas the Orowan mechanism is strongly dependent on particle size. The microstructural change during this transition from shearing to looping controlled deformation occurs because the "laminar" dislocation flow for the former differs from the turbulent plastic flow for non-deformable particles. The high density of dislocation loops formed due to Orowan mechanism results in a high rate of strain hardening[80,82].

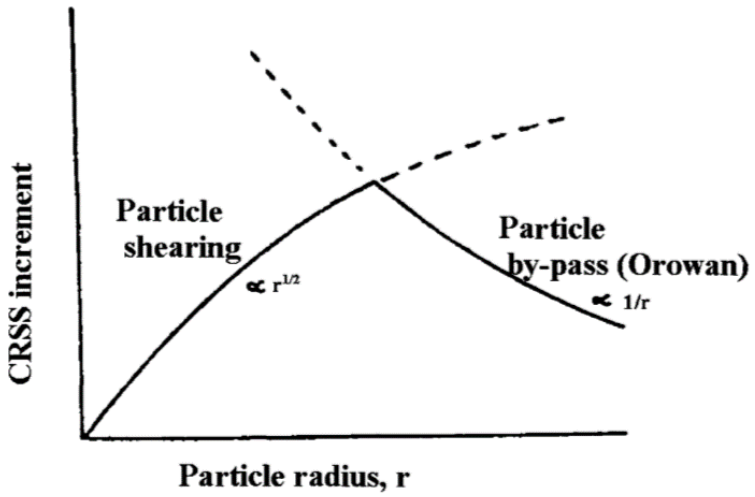

Figure 3.13 – CRSS increment versus particle radius for the mecanisms of (a) particle shearing and (b) particle by-pass (Orowan).
[MARTIN, 1998[80]]

Earlier studies[83–86] considered that the Orowan mechanism governed the interaction between dislocations and precipitates in Mg alloys. However, more recent studies have shown that the basal dislocations can easily shear the precipitates[68,87–91]. Cepeda-Jiménez, Castillo-Rodríguez, and Pérez-Prado (2019)[88] have observed a substantial shearing of MN11 alloy precipitates by basal dislocations, which is the proposed reason for the low precipitation hardening of this alloy. The precipitates studied were Mg_xNd_y plates, perpendicular to the basal plane. The high shearability is attributed to the high degree of coherency between the precipitates and matrix, and also to the small size of precipitates, which facilitates the cutting by the basal dislocations.

Despite having a significant amount of studies on the interaction of precipitates with basal dislocations, there is little research on this interaction with non-basal dislocations. Recently, Wang, Cepeda-Jiménez, and Pérez-Prado (2020)[92] investigated the particle-dislocations interactions (basal and non-basal) of an MN11 alloy to understand its low precipitation hardening. Figure 3.14 shows an example of how high-resolution transmission electron microscopy (HRTEM) provides a visualization of the precipitate structure on an atomic resolution. The investigated precipitate has a prismatic plate morphology, suggesting that they correspond to the β'' phase, which has an ordered hexagonal $D0_{19}$ lattice[56], and it is located on a well-oriented crystal for basal slip. The

fast Fourier transform (FFT) diffractograms confirm the presence of the β'' phase, and the images show a very high coherence between the matrix and the well-oriented for basal slip particles, which indicate the precipitate is prone to be cut by basal dislocations.

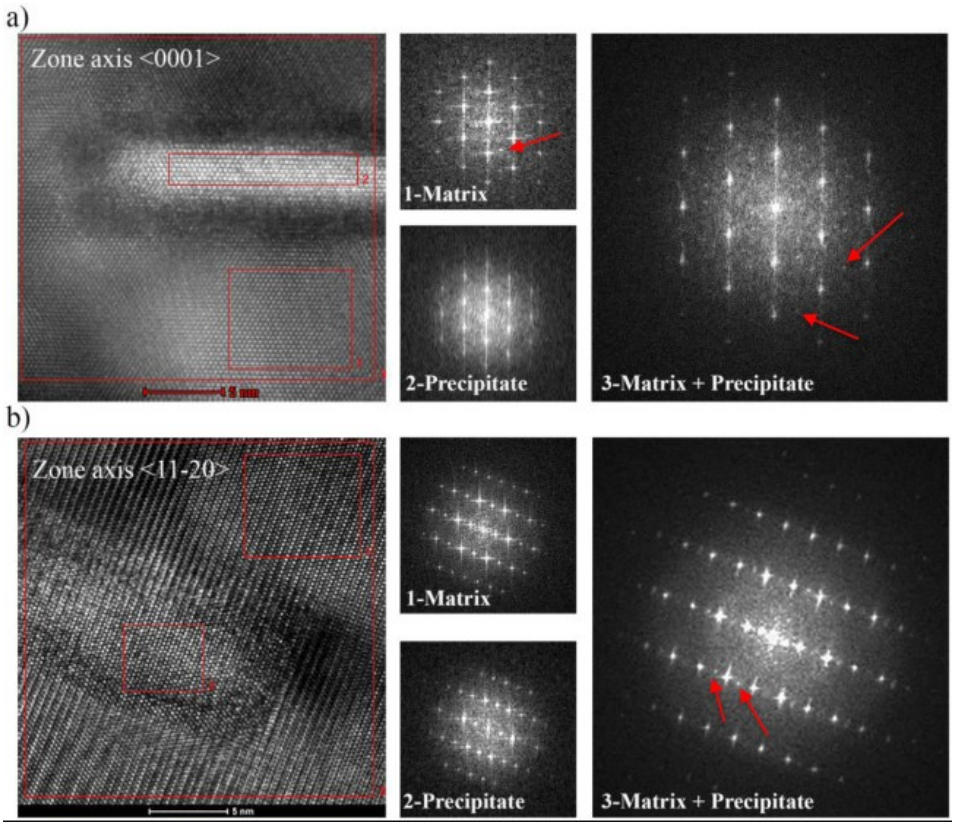

Figure 3.14 – HRTEM micrographs of a plate precipitate within the Mg matrix, viewed along the (a) <0001> and (b) <11$\bar{2}$0> zone axes. For both cases, the FFT diffractograms corresponding to (1) the matrix, (2) the precipitate, and (3) matrix + precipitate are included next to the corresponding high-resolution images. Some of the $D0_{19}$ superlattice reflections are highlighted with red arrows.
[WANG, CEPEDA-JIMÉNEZ & PÉREZ-PRADO, 2020[92]]

The pyramidal ⟨**c** + **a**⟩ dislocations can interact with the precipitates in two ways: by shearing along the precipitate pyramidal planes, or by Orowan mechanism. The shearing only occurs when there is a good alignment between the slip plane of the incoming matrix dislocation and the outgoing pyramidal plane from the precipitate. On the other hand, if there is a small geometric compatibility between the pyramidal dislocation and the precipitate pyramidal planes, the dislocation can circumvent the particle by an Orowan looping mechanism[92].

The Mg_xNd_y and Mn precipitates behave in very different ways concerning the dislocation-particle interaction, as is evident in this bright-field (BF) TEM micrograph depicted in Figure 3.15. The image illustrates the microstructure of the micropillar used in the experiments after compression strain. The Mn precipitates exhibit a dark black contrast, whereas the Mg_xNd_y precipitates appear as gray shapes. While the plate Mg_xNd_y precipitates went through an intense shearing, even breaking into small fragments, those of Mn hardly deformed. Due to the low geometric compatibility between the Mn precipitates and the matrix, it is rare to observe Mn-rich particles being sheared by basal and pyramidal dislocations. Therefore, the Mn precipitates may act as hard particles, not undergoing significant deformation[92].

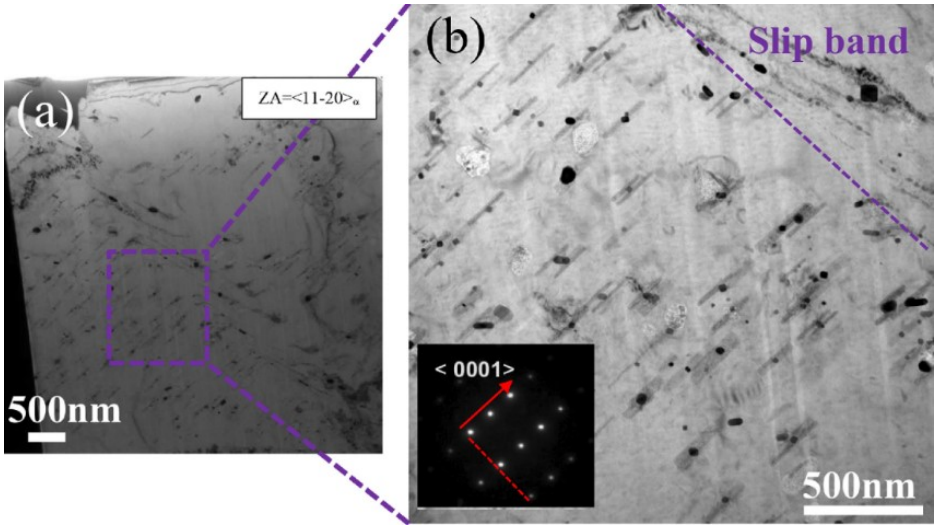

Figure 3.15 – TEM BF micrograph illustrating a cross-section of a deformed micropillar (a), and an enlarged view of the region enclosed within the purple rectangle (b). A well-defined slip band, where significant particle shearing and fracture can be noticed, is highlighted. The orientation of the basal plane is indicated in the selected area diffraction (SAD) diagram with the red dotted line. The zone axis is <11-20>$_\alpha$. [WANG, CEPEDA-JIMÉNEZ & PÉREZ-PRADO, 2020[92]]

3.2 Severe plastic deformation (SPD)

Severe plastic deformation (SPD) has been generating interest from scientists since it enables the production of materials with an exceptional grain refinement, usually in the submicrometer or nanometer scale, known as ultrafine-grained (UFG). Such fine grain sizes cause significant changes in the properties of materials. Differently from other more traditional metalworking processes, such as rolling and extrusion, SPD can impose a very high plastic strain on a bulk material without mechanical significant damage, cracks, and alteration of its overall dimensions[93].

The most common methods of SPD are equal-channel angular pressing (ECAP) and high-pressure torsion (HPT). However, using ECAP on Mg alloys may not be recommended, as it generates structural damage to the material at room temperature, such as cracking and fracture[94–96]. Otherwise, HPT applies a high hydrostatic pressure on the material, which prevents the propagation of cracks. This deformation method has succeeded in the processing of various Mg-alloys, such as AZ31[97], AZ80[98], and AZ91[99].

3.2.1 *Principles of high-pressure torsion (HPT)*

The HPT process is schematized in Figure 3.16. The sample in the form of a disk is placed between two anvils and is subjected to a compressive pressure P in the order of several GPa, usually at room temperature. At the same time, the lower support imposes a torsional strain through rotation, deforming the disk by shear due to the surface friction forces[100].

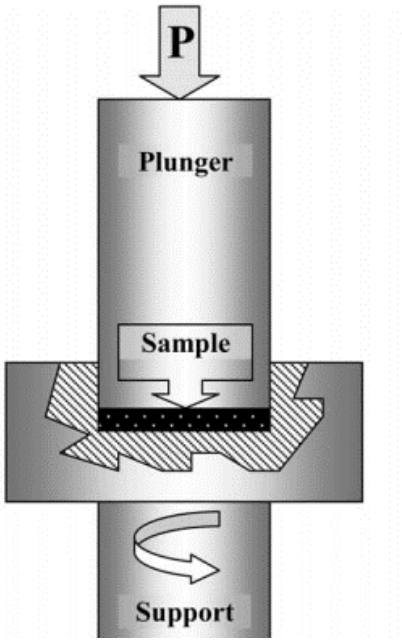

Figure 3.16 - Schematic illustration of HPT processing
[ZHILYAEV et al., 2003[100]]

Inhomogeneity is intrinsic to the HPT process. When a disk is processed by HPT, the equivalent von Mises strain, ε_{eq}, is calculated according to the following equation([101]):

$$\boldsymbol{\varepsilon_{eq} = \frac{2\pi N r}{h\sqrt{3}}} \tag{3.2}$$

where *N* is the number of turns, and *r* and *h* are the radius and the thickness of the disk, respectively.

3.2.2 *Studies on the influence of HPT on the microstructure of Mg alloys*

The heterogeneous character of HPT can be observed microstructurally, as shown in Figure 3.17, which has optical micrographs of an AZ61 alloy at the center, middle, and edge of the disks for a different number of turns[102]. It is evident that the further away from the center of the disk, the more deformation the sample undergoes, as provided by Equation 3.2. However, when the number of turns increases, this microstructural difference between the center and the edge becomes insignificant, which is observed in other studies[100,103–106]. Zhilyaev et al. (2003)[100] proposed a simple model to explain this phenomenon, based on the occurrence of a repetitive shearing transfer at adjacent

positions within the disk since the deformation in a favorable area causes local hardening. This evolution towards a more homogeneous structure is also predicted by the modeling of strain gradient plasticity using a solid mechanics approach[107,108]. Therefore, it is possible to achieve relatively homogeneous microstructures with HPT when the number of turns and the applied pressure are sufficiently high.

HPT significantly reduces the grain size, and this is related to the high density of defects generated during the process caused by the application of high hydrostatic pressure in combination with large shear strains. The grain refinement during SPD is a multi-step process, and it is illustrated in Figure 3.18[109]. Initially, the dislocations are randomly distributed within the grain (Figure 3.18a), and to reduce the strain energy associated with this configuration, the dislocations group together to form elongated cells (Figure 3.18b). With further deformation and increasing misorientation, these cells transform into subgrains (Figure 3.18c), whose boundaries are defined as low-angle grain boundaries (LAGBs). The plastic deformation that occurs in these subgrains causes them to break up (Figure 3.18d), and eventually they break into approximately equiaxed micrograins, whose boundaries are defined as high-angle grain boundaries (HAGBs).

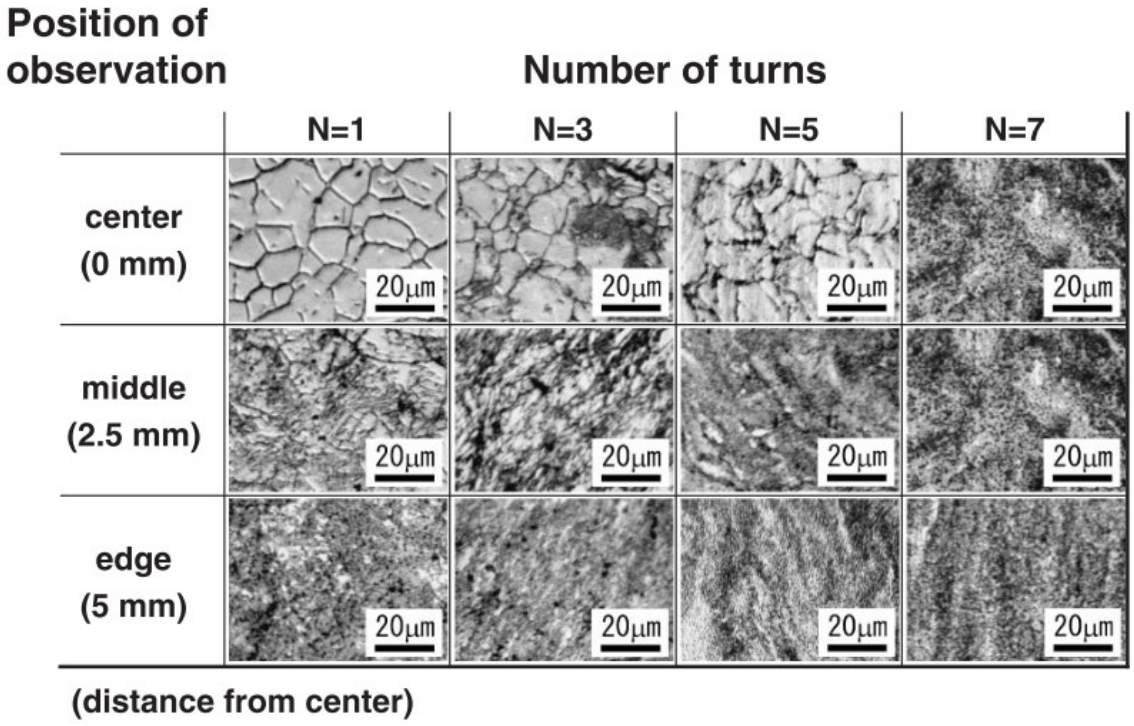

Figure 3.17 – Optical micrographs showing the microstructures of an AZ61 alloy at the center, half-way position and edge of each disk after N = 1, 3, 5, and 7 HPT turns.
[HARAI et al., 2008[102]]

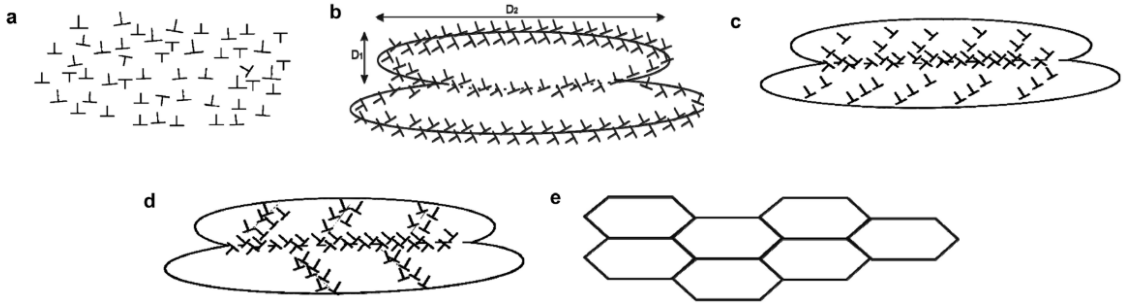

Figure 3.18 – Schematic illustration of microstructural evolution during SPD. (a) Homogeneous distribution of dislocations; (b) elongated cell formation; (c) dislocations blocked by subgrain boundaries; (d) break up of elongated subgrains; and (e) reorientation of subgrain boundaries and formation of ultrafine grain size.
[Adapted from MISHRA et al., 2008[109]]

However, several studies[110–115] show that the mechanism of grain refinement of Mg and its alloys during SPD at high temperatures is significantly distinct from other metals. Differently from fcc metals, the dislocation structures and subgrain boundaries of HPT-processed Mg alloys are not formed within coarser grains in the early stages of

deformation. Instead, grains are refined by dynamic recrystallization, in which new grains are nucleated along the boundaries of the original grains, occurring in a necklace pattern, as shown in Figure 3.19. Because of it, a multi-modal grain size distribution is reported at low strain levels[116,117]. Experimental data indicate the mechanism of Mg grain refinement subjected to SPD processing at room temperature is similar to that found at high temperatures[118].

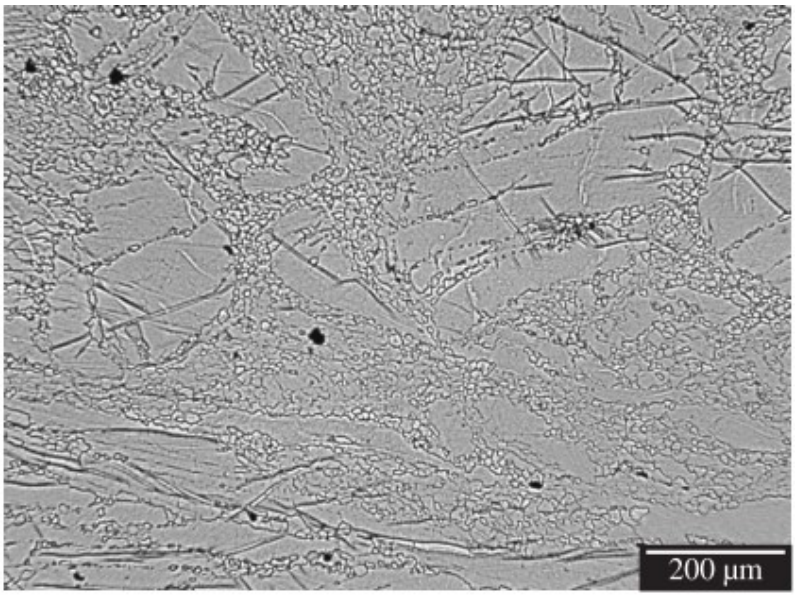

Figure 3.19 – Optical micrograph of a HPT-processed Mg showing its grain structure at the end of the deformation zone. The fine grains are distributed in a necklace pattern around areas of unrefined coarse grains.
[POGIALLI et al., 2012[115]]

Another microstructural change caused by SPD is the fragmentation of second phase particles since the large strain and stress during HPT induce the breaking of hard precipitates. As seen in previous chapters, a homogeneous distribution of fine particles inside the grain improves the strength, and can also improve the thermal stability of the microstructure by inhibiting grain growth[20,73–75]. As an example, Figure 3.20 shows the size reduction of non-shearable precipitates with increasing strain of a Al-Mg alloy processed by HPT[119]. To the best of my knowledge, there are no studies of a Mg-Mn-Nd alloy processed by HPT. Thus, it will be interesting to notice if HPT can break the hard Mn particles, and what would be the consequences of this fragmentation on the mechanical properties of the alloy.

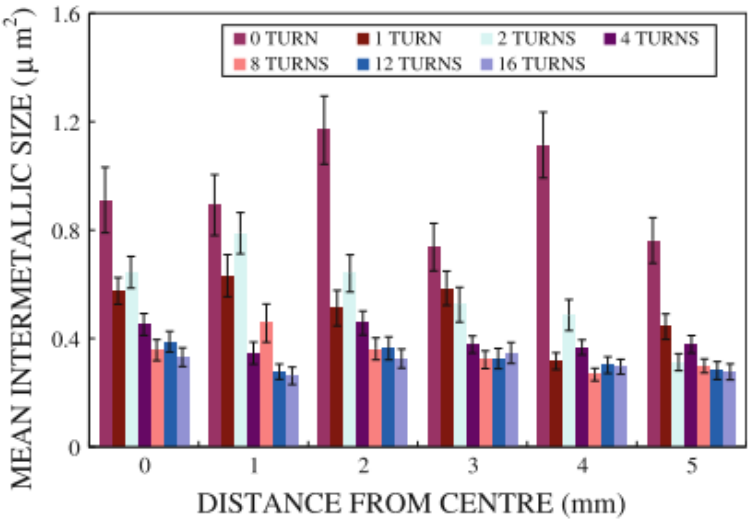

Figure 3.20 – Measured particle size of Al–1wt%Mg alloy for samples processed up to 16 turns by HPT.
[CRUMP, QIAO & STARINK, 2012[119]]

The formation of supersaturated solid solutions of elements whose mutual solubility is extremely low at room temperature can be induced by mechanical alloying during HPT[120,121]. Sauvage, Wetscher, and Pareige (2005)[120] used SPD to produce a non-equilibrium solid solution of two non-miscible elements[122], Fe and Cu, in a bulk specimen. This alloying occurs because SPD induces the deformation and fragmentation of Fe into small particles with a nanoscale tip. According to the Gibbs-Thomson effect, these fine precipitates are associated with a higher free energy due to the increase of precipitate-matrix surface area, making the particles unstable and thus causing them to dissolve into the matrix[123]. Since the interdiffusion of Fe in Cu is negligible at low temperatures[124], the HPT must promote at least one diffusion mechanism. Several features could improve the atomic mobility, such as atomic transport along grain boundaries (GBs) and diffusion along dislocations[125–127]. However, even though there is an enormous proportion of GB in nanoscale systems, the diffusion occurring in these GBs is remarkably low due to the high pressure applied to the specimen during HPT, according to phase diagrams[126,128]. Also, despite the high dislocation density produced by SPD, these defects are mostly located along GBs[93], and the strain rate during HPT is sufficient to make the dislocations move free of solute atmospheres[129]. As the mechanisms mentioned above are unlikely to clarify the mechanical alloying caused by SPD, the

proposed explanation for the enhanced diffusion is the increase of the mobile vacancy concentration. The compressive strain imposed by HPT and the nanoscale particles significantly lower the vacancy formation energy, increasing the concentration of vacancies[130,131]. The high strain also lowers the vacancy migration energy[132], and thus the mobile vacancies generated during HPT increase the diffusion coefficient of Fe in Cu[133], enabling the mechanical alloying.

The solute elements of a supersaturated solid solution may be redistributed during SPD through segregation to defects and formation of clusters and precipitates. These phenomena may significantly affect properties[134], such as strength[135–140] and thermal stability[141–143], which are critical issues for a broader use of UFG materials. The grain boundary segregation, also known as nanosegregation, occurs because the solute atoms accumulate at GBs to reduce the total energy of the system. In non-equilibrium conditions, as in irradiated materials, the solute atoms interact with the excess of vacancies in the material, and the GBs act as sinks for the vacancy-solute pairs. Thus, the flow of vacancies to the GBs increases the solute concentration around the boundaries in order to preserve their thermal equilibrium value[134,144,145].

Sauvage et al. (2014)[146] studied the mechanisms of precipitation and segregation in a Al-Mg alloy processed by HPT. They observed with SEM and APT that Mg uniformly segregates to GBs at higher temperatures, whereas, at room temperature, Mg is in the form of nanoclusters homogeneously distributed in the matrix, and not only along GBs. HPT is responsible for the increased mobility of the solute atoms, as it induces the formation of dislocations and vacancies. Nevertheless, they concluded that dislocations do not play a significant role in the movement of Mg atoms, since the high strain imposed by HPT prevents dislocations from dragging atoms[129]. Instead, they are dragged by the vacancies toward GBs at room temperature, as Mg atoms are strongly coupled to these defects because of the positive binding energy between them. The vacancies recombine and annihilate at the GBs, and the remaining Mg atoms form segregation or clusters around the boundaries. This mechanism is very similar to that of non-equilibrium segregation resulting from irradiation[134,144,145], and it is represented in Figure 3.21.

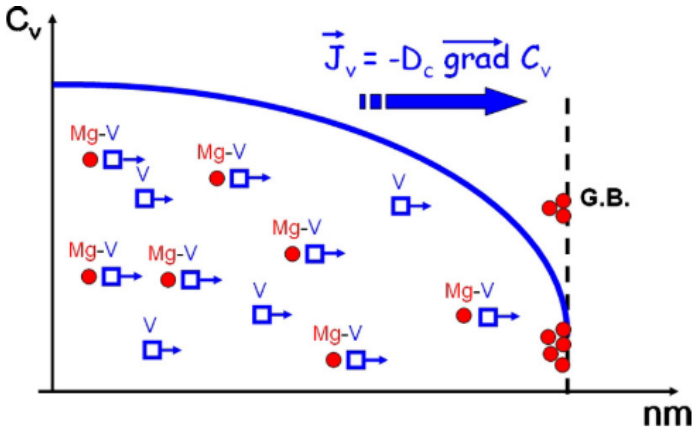

Figure 3.21 - Schematic representation of the diffusion of Mg toward GBs assisted by the vacancy flux (J_v).
[SAUVAGE et al., 2014[146]]

Numerous studies have reported segregation in Mg alloys[139,140,147–150]. Robson et al. (2016)[147] have investigated the influence of RE atoms segregation in the texture change. They used HAADF-STEM and EDS mapping and determined that the Mg-Y alloy, where the solubility and composition of Y are relatively high, showed the RE texture change effect. However, the Nd atoms did not segregate, since they were most present in insoluble particles. Previously, Robson (2014)[151] had shown that the tendency for an element to segregate to GBs under equilibrium conditions can be predicted by the Langmuir–McLean model[152]. In this model, stronger segregation is achieved with a high atomic size difference between solvent and solute atoms. This misfit causes a lattice distortion, and the solute segregates at defect sites to minimize the associated elastic strain. According to the model, Nd should have an even greater tendency to segregate than Y, but STEM revealed Nd-Fe particles that reduce the availability of Nd in the matrix. Therefore, for Nd to segregate, a high solubility and a fast diffusion rate are also necessary. These factors are provided by HPT since the energy barrier for diffusion is reduced by the high density of defects generated in the process, even at room temperature. Horky et al. (2019)[148] studied the origin of the exceptional strengthening of HPT-processed Mg-Zn-Ca alloys with subsequent heat treatment. Although they observed segregations of Zn and Ca through APT, they concluded that these segregations are not the main responsible for the strengthening, since different thermal treatments causing different amounts of segregation did not change the hardness. Instead, they relate the increase in strength to the high concentration of vacancies during the HPT process, which

leads to the formation of vacancy agglomerates and dislocation loops in the basal plane. Basha et al. (2016, 2017)[149,150] observed segregations of Zn in HPT-processed Mg–Zn–Y alloys by using HAADF imaging and EDS mapping. They concluded that Zn atoms are transported by the SPD-induced vacancy flux in case of HPT at room temperature, whereas the Zn atoms are dragged by equilibrium vacancies and dislocations on extrusion at 573 K since the strain rate is smaller than in HPT[129]. Sun et al. (2018)[139,140] showed evidence of segregations of Gd, Y, and Zn in a Mg alloy using techniques such as HAADF, EDS, and XRD. They suggested that the outstanding strengthening was due to the combined effects of solute segregation, grain refinement, and high dislocation density caused by HPT processing.

3.2.3 *Studies on the influence of HPT on the mechanical properties of Mg alloys*

Some studies have been investigating the effect of the microstructural changes during HPT in mechanical properties such as hardness and strength. Bourezg et al. (2018)[153] studied Mg-Nd and Mg-Ce alloys to examine the influence of HPT on their microhardness. With only a ½ turn, a sharp increase in hardness was observed in Figure 3.22. According to Qiao et al. (2014)[154], dislocation hardening and grain size strengthening are insufficient to explain this rise, since the grain refinement and dislocation density at this level of strain is limited. One possible explanation for this is the reorganization of the basal planes to be parallel to the shear direction, instead of being randomly organized as in the as-cast condition. Between 1 and 10 turns, the change in hardness is very subtle, and the reasons for this are the saturation of grain subdivision, the dislocation density, and also the dynamic recovery that happens in HPT processed materials even at room temperature. The generation of dislocations reaches a steady-state, and they are also being annihilated in recovery[155]. The hardening rate of Mg-Nd was higher than the one of Mg-Ce, and the maximum values of hardness achieved are, respectively, ~65 and ~96 HV. This may be due to precipitate/dislocation effects and residual solute/dislocation. Another reason is the influence of the characteristics of Mg_xRE_y phases, such as their size, morphology, and distribution. In the literature, there is very little information about such correlations, especially after SPD, and thus it is necessary a further investigation[153].

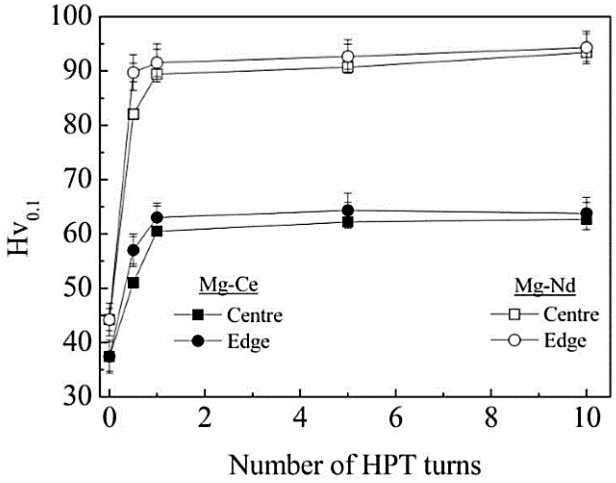

Figure 3.22 – Evolution of Vickers microhardness with the number of HPT turns of Mg-1.43%wtNd and Mg-1.44%wtCe alloys.
[BOUREZG et al., 2018[153]]

In a study conducted by Xu et al. (2015)[156], microhardness tests were performed to evaluate the mechanical properties of an AZ31 magnesium alloy processed by HPT. The variation of microhardness as a function of distance from the centers of the disks is illustrated in Figure 3.23. The lower dashed line displays the initial average hardness ~62 HV for the annealed sample without HPT processing. The hardness measurements increased significantly with the number of turns, and a heterogeneity in the values was also observed – while the edges of the disk have hardness values oscillating from ~120 to ~132 HV, the center has a much lower value of ~85 HV The hardness measurements in the central region rise gradually with the number of turns until a saturation is reached at ~125 HV after 10 turns.

The development of homogeneity in HPT processing was investigated in more detail with a color-coded microhardness mapping in Figure 3.24. A gradual evolution towards higher values of hardness and homogeneity is evident when the number of turns increases, being consistent with the results expressed in Figure 3.23.

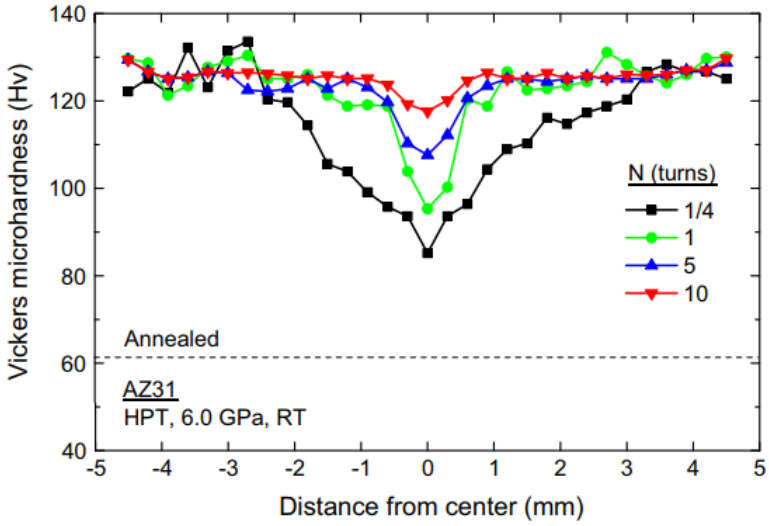

Figure 3.23 – Vickers microhardness across diameters of disks after HPT processing of an AZ31 alloy through various numbers of turns.

[XU et al., 2015[156]]

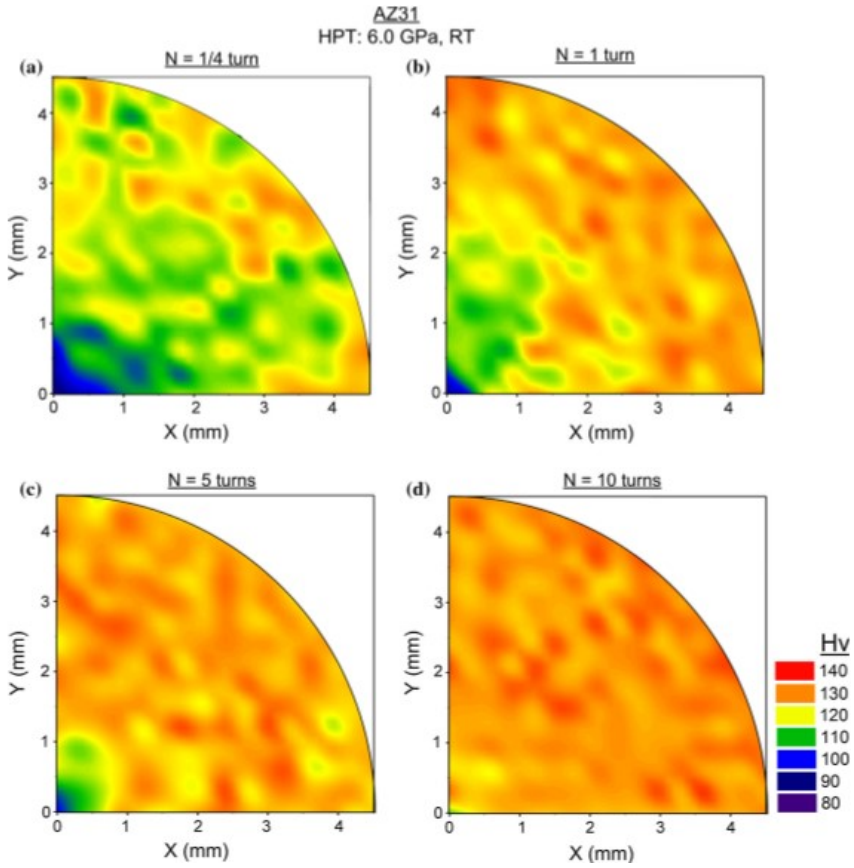

Figure 3.24 - The variations in microhardness over one-quarter areas of AZ31 disks processed by HPT through (a) 1/4, (b) 1, (c) 5, and (d) 10 turns.

[XU et al., 2015[156]]

Heterogeneous hardness values in an HPT processed EZ33A alloy were also studied by Bryla et al. (2018)[157]. A color-coded plot of hardness distribution for a different number of turns is illustrated in Figure 3.25. The average hardness is shown below each sample.

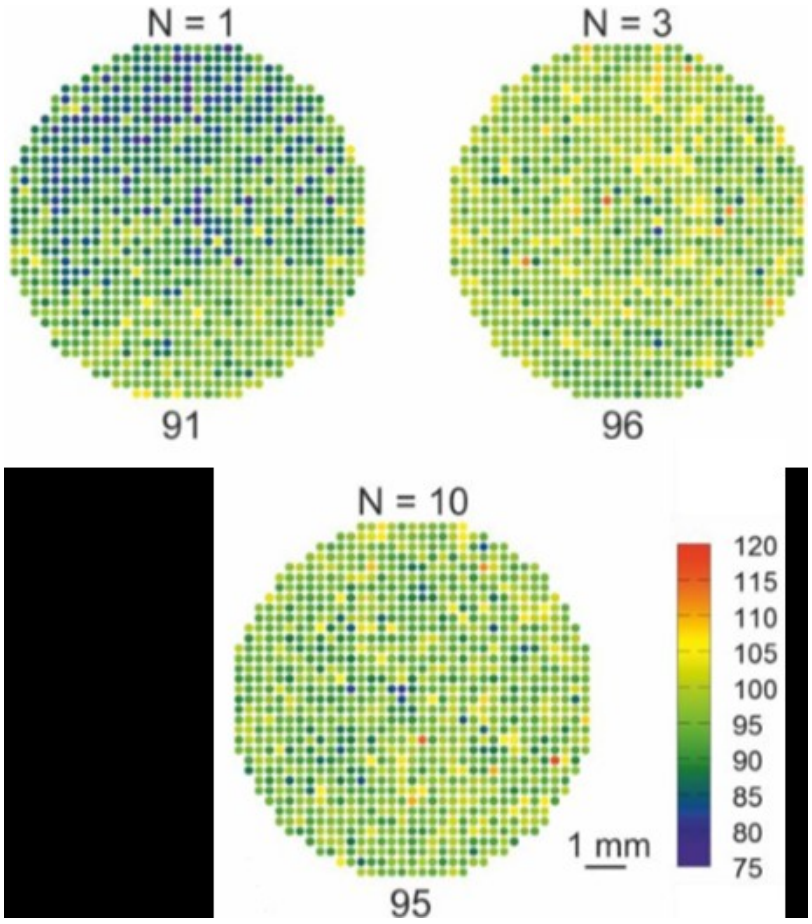

Figure 3.25 – Hardness distribution with average values of EZ33A disks processed by HPT through (a) 1, (b) 3, and (c) 10 turns.
[BRYLA et al., 2018[157]]

As expected, hardness increased with the number of turns – the as-cast material had approximately 60 HV, and after the HPT processing hardness was raised to 90-95 HV. With only 1 turn, heterogeneity is evident between the two halves of the disk. The disk submitted to 10 turns is not significantly different from the disk with 3 turns, perhaps slightly more homogeneous.

Tensile tests were also performed, and their stress-strain curves for as-cast and after HPT processing are presented in Figure 3.26. The yield strength and ultimate tensile strength of the HPT processed alloy were greatly improved from the as-cast material. Ductility was also improved, but in the case of 10 turns, it decreases due to the diminishing number of large grains surrounding UFG colonies, facilitating the crack propagation. The study concluded that bimodal grain size distribution and the fragmentation and redistribution of brittle $(Mg,Zn)_{12}Ce$ phase were the causes of the improvement of strength and ductility.

Investigating the effect of the HPT process on mechanical properties is essential to determine the best parameters for the most optimized alloy. In literature, there is little research on Mg-RE alloys processed by HPT. Therefore, it is necessary to study and characterize them thoroughly.

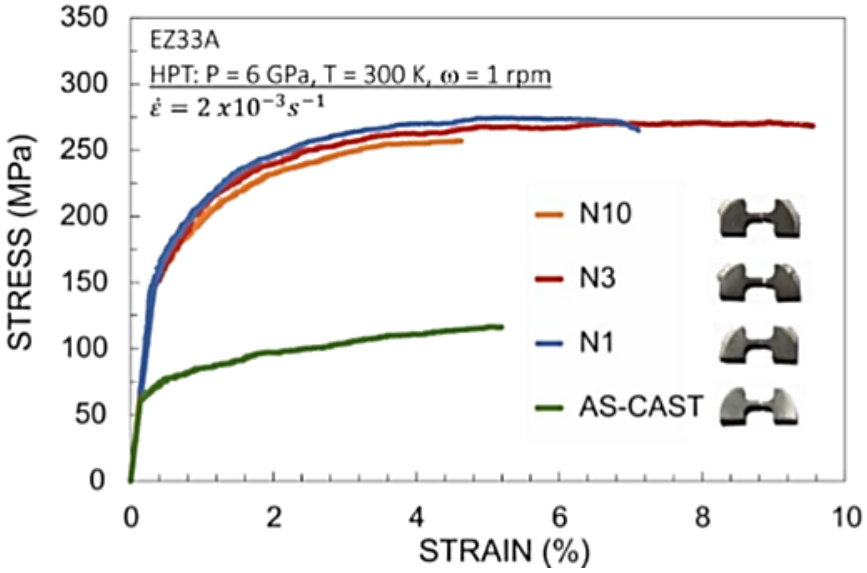

Figure 3.26 - Tensile stress-strain curves for the as-cast and HPT-processed EZ33A alloy. [BRYLA et al., 2018[157]]

3.3 Scanning transmission electron microscopy (STEM)

The scanning transmission electron microscope (STEM) is a key tool for the study of UFG materials since it provides information on the electronic structure and elemental composition to the atomic resolution. The operation principle of STEM is the same as the normal scanning electron microscope (SEM), which consists in the focusing of the

electron beam into a small spot that scans over the sample while a signal is collected to generate an image. The difference between the techniques is that STEM requires a thin sample so that transmission modes of imaging are used[158].

The components of a STEM are illustrated in Figure 3.27. A source emits electrons that are accelerated and focused on a point on the sample by a series of condenser lenses and an objective lens. The maximum angle of illumination in the incident probe is limited by an objective aperture, which is scanned across the specimen by the scan coils. There are a variety of detectors to collect different parts of the diffraction pattern and form images, such as the annular dark-field (ADF), that gathers scattered electrons in the surrounds of the transmitted beam, and a BF detector, that intercepts the beam[158]. Figure 3.28 illustrates the different types of detectors for each signal.

.

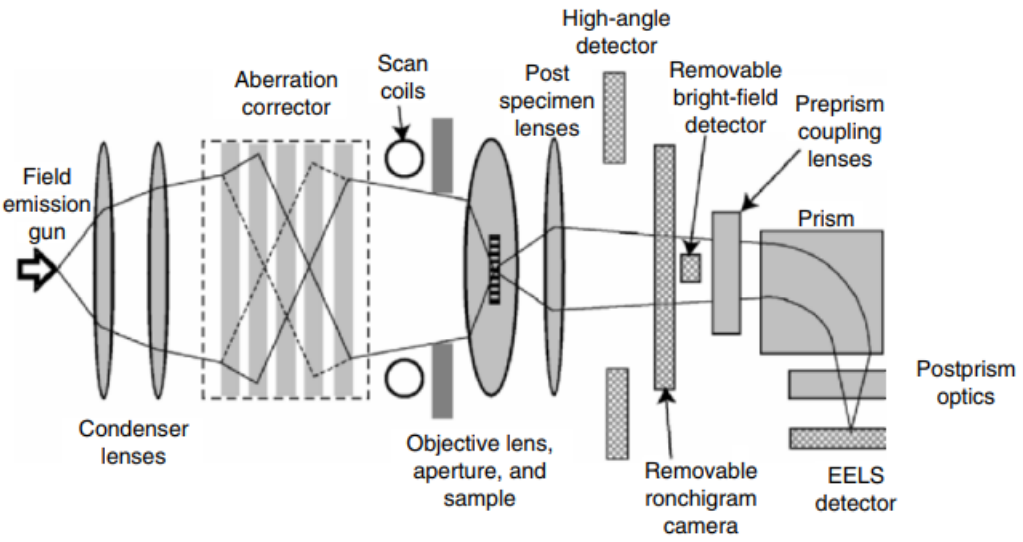

Figure 3.27 – Illustration of the components of a high-resolution STEM. [PENNYCOOK et al., 2007[158]]

3.3.1 *High-angle annular dark-field imaging (HAADF)*

High-angle annular dark-field (HAADF) is an imaging STEM technique recognized for having a high sensitivity to variations in the atomic number (Z) of the sample. Its image, known as Z-contrast image, is produced by a very high angle, incoherently **coherent** Rutherford scattered electrons, as observed in Figure 3.28[159].

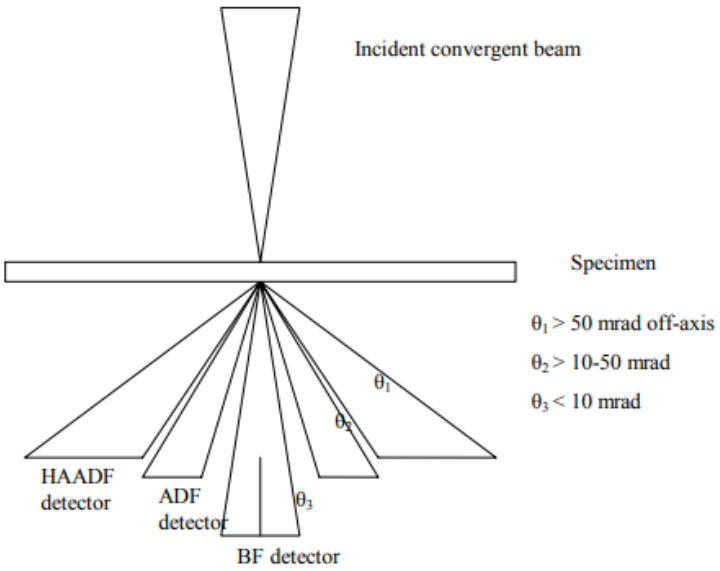

Figure 3.28 – STEM BF, ADF and HAADF detectors and their angular ranges. [PETROVA, 2007[159]]

The brightest regions in a Z-contrast image are the ones with higher Z, due to the greater signal received by the HAADF. The electrostatic interactions are stronger between the electron beam and the nucleus, and therefore more electrons are scattered at higher angles. Because of this high dependence on Z, HAADF is an interesting method for identifying small areas of an element with a high Z in a matrix of a material with lower Z, such as precipitates. For that reason, this technique is being used in studies of Mg-RE alloys.

Sun et al. (2018)[139] investigated a nanostructured Mg-8.2Gd-3.8Y-1.0Zn-0.4Zr (wt.%) alloy produced by solution treatment followed by HPT using HAADF-STEM and elemental mapping. An extensive solute segregation along grain boundaries was revealed by those techniques, as shown in Figure 3.29.

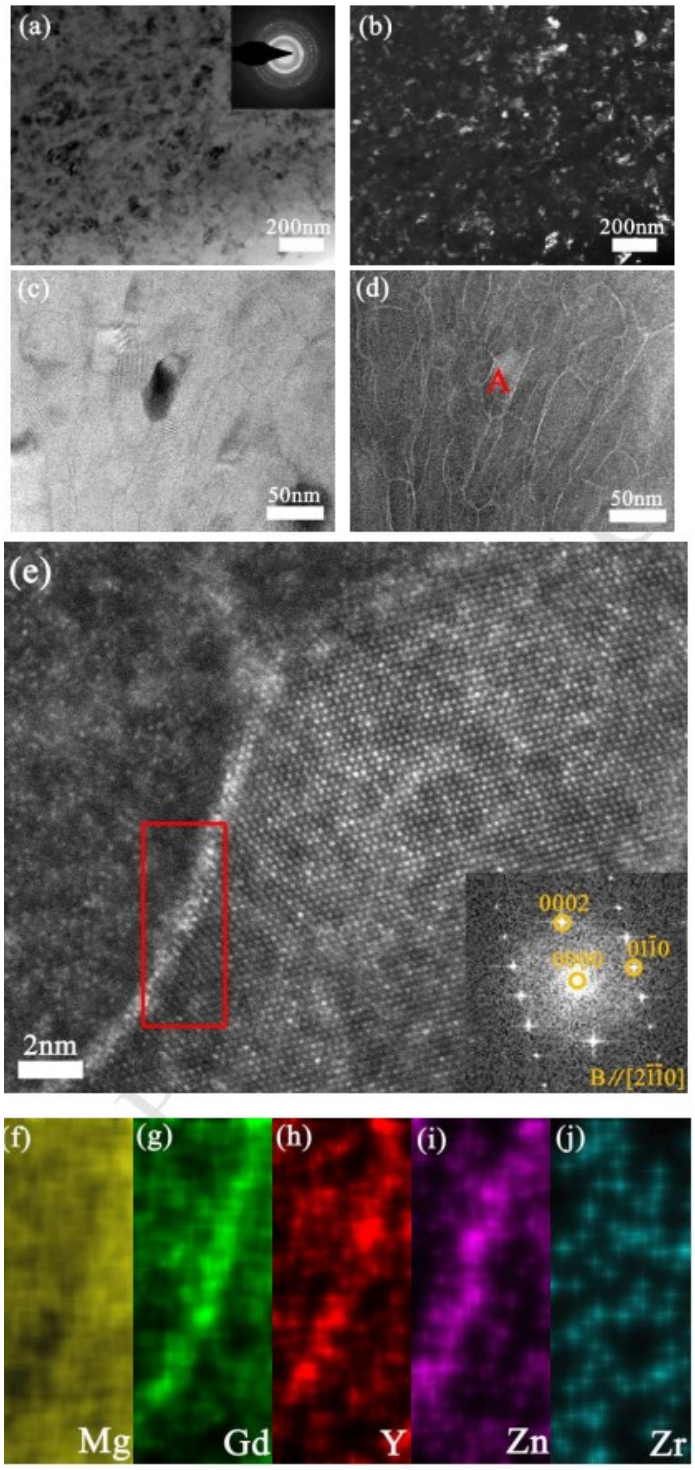

Figure 3.29 - Microstructure of the HPT-processed sample (a) TEM bright-field image and corresponding SAD pattern; (b) TEM dark-field image; (c) A high magnification TEM BF image; (d) HAADF-STEM image; (e) Atomic-resolution HAADF-STEM image of grain A marked in (d) and corresponding FFT image, and elemental mappings of red rectangular region marked in (e): (f) Mg; (g) Gd; (h) Y; (i) Zn; (j) Zr.

[SUN et al., 2018[121]]

REFERENCES

[1] NATIONAL RESEARCH COUNCIL (U.S.), Assessment of Technologies for Improving Light Duty Vehicle Fuel Economy. Washington, D.C.: *The National Academies Press*, 2010.

[2] GROVES, G. W.; KELLY, A. Independent slip systems in crystals. *The Philosophical Magazine: A Journal of Theoretical Experimental and Applied Physics*, v. 8, n. 89, p. 877-887, 1963.

[3] YOO, M. H. Slip, Twinning, and Fracture in Hexagonal Close-Packed Metals. *Metallurgical Transactions A*, v. 12, n. 3, p. 409–418, 1981.

[4] WU, Z.; CURTIN, W. A. The origins of high hardening and low ductility in magnesium. *Nature*, v. 526, p. 62–67, 2015.

[5] WU, Z. et al. Mechanistic origin and prediction of enhanced ductility in magnesium alloys. *Science*, v. 359, n. 6374, p. 447–452, 2018.

[6] SANDLÖBES, S. et al. Basal and non-basal dislocation slip in Mg – Y. *Materials Science & Engineering A*, v. 576, p. 61–68, 2013.

[7] SANDLÖBES, S. et al. The relation between ductility and stacking fault energies in Mg and Mg–Y alloys. *Acta Materialia*, v. 60, p. 3011-3021, 2012.

[8] PEI, Z. et al. Rapid theory-guided prototyping of ductile Mg alloys: From binary to multi-component materials. *New Journal of Physics*, v. 17, n. 9, 2015.

[9] REED-HILL, R. E. *Princípios de metalurgia física*. 2. ed. Rio de Janeiro: Guanabara Dois, 1982.

[10] KOCKS, U. F.; WESTLAKE, D. G. The importance of twinning for the ductility of CPH polycrystals. *Transactions of the Metallurgical Society of AIME*, v. 239, p. 1107-1109, 1967.

[11] HUTCHINSON, J. W. Creep and plasticity of hexagonal polycrystals as related to single crystal slip. Metallurgical Transactions A, v. 8, n. 9, p. 1465–1469, 1977.

[12] BARNETT, M. R. Twinning and the ductility of magnesium alloys. Part II. “Contraction” twins. *Materials Science and Engineering A*, v. 464, n. 1–2, p. 8–16, 2007.

[13] LENTZ, M. et al. Grain size effects on primary, secondary, and tertiary twin development in Mg-4 wt pct Li (-1 wt pct Al) alloys. *Metallurgical and Materials Transactions A: Physical Metallurgy and Materials Science*, v. 45, n. 11, p. 4737–4741, 2014.

[14] JAIN, A. et al. Grain size effects on the tensile properties and deformation mechanisms of a magnesium alloy, AZ31B, sheet. *Materials Science and Engineering A*, v. 486, n. 1–2, p. 545–555, 2008.

[15] BARNETT, M. R. et al. Necking and failure at low strains in a coarse-grained wrought Mg alloy. *Scripta Materialia*, v. 59, n. 10, p. 1035–1038, 2008.

[16] ZHAO, C. et al. Strain hardening behavior of Mg–Y alloys after extrusion process. *Journal of Magnesium and Alloys*, v. 7, n. 4, p. 672–680, 2019.

[17] ZHAO, C. et al. Strain Hardening Behavior in Mg–Al Alloys at Room Temperature. *Advanced Engineering Materials*, v. 21, n. 3, p. 1–10, 2019.

[18] AFRIN, N. et al. Strain hardening behavior of a friction stir welded magnesium alloy. *Scripta Materialia*, v. 57, n. 11, p. 1004–1007, 2007.

[19] CHAI, Y. et al. Role of Al content on the microstructure, texture and mechanical properties of Mg-3.5Ca based alloys. *Materials Science and Engineering A*, v. 730, p. 303–316, 2018.

[20] CALLISTER, W. D.; RETHWISCH, D. G. *Materials science and engineering*: an introduction. 10. ed. Hoboken: Wiley, 2018.

[21] ZHAO, C. et al. Effect of Sn content on strain hardening behavior of as-extruded Mg-Sn alloys. *Materials Science and Engineering A*, v. 713, p. 244–252, 2018.

[22] ZHAO, C. et al. Strain hardening of as-extruded Mg-xZn (x = 1, 2, 3 and 4 wt%) alloys. *Journal of Materials Science and Technology*, v. 35, n. 1, p. 142–150, 2019.

[23] IMANDOUST, A.; BARRETT, C. D.; EL KADIRI, H. Effect of rare earth addition on $\{10\bar{1}2\}$ twinning induced hardening in magnesium. *Materials Science and Engineering A*, v. 720, p. 225–230, 2018.

[24] HADORN, J. P. et al. Role of solute in the texture modification during hot deformation of Mg-rare earth alloys. *Metallurgical and Materials Transactions A*, v. 43, n. 4, p. 1347–1362, 2012.

[25] STANFORD, N. et al. Effect of microalloying with rare-earth elements on the texture of extruded magnesium-based alloys. *Scripta Materialia*, v. 59, n. 7, p. 772–775, 2008.

[26] NIE, J. F. et al. Periodic segregation of solute atoms in fully coherent twin boundaries. *Science*, v. 340, n. 6135, p. 957–960, 2013.

[27] VAN VLACK, L. H. *A Textbook of Materials Technology*. Boston: Addison-Wesley, 1973.

[28] YU, H. et al. Hall-Petch relationship in Mg alloys: A review. *Journal of Materials Science and Technology*, v. 34, n. 2, p. 248–256, 2018.

[29] ARMSTRONG, R. et al. The plastic deformation of polycrystalline aggregates. *Philosophical Magazine*, v. 7, n. 73, p. 45–58, 1962.

[30] LI, J. C. M. Petch relation and grain boundary sources. *Transactions of the Metallurgical Society of AIME*, v. 47, p. 239–247, 1963.

[31] HALL, E. O. The deformation and ageing of mild steel: III discussion of results. *Proceedings of the Physical Society. Section B*, v. 64, p. 747, 1951.

[32] DOIPHODE, R. L. et al. Grain growth in calibre rolled Mg-3Al-1Zn alloy and its effect on hardness. *Journal of Magnesium and Alloys*, v. 3, n. 4, p. 322–329, 2015.

[33] BALÍK, J. et al. Modeling of the work hardening in magnesium alloy sheets. *International Journal of Plasticity*, v. 76, p. 166–185, 2016.

[34] KASSNER, M. E.; PEREZ-PRADO, M. T. *Fundamentals of Creep in Metals and Alloys.* 1. ed. Oxford: Elsevier, 2004.

[35] Pande C.S.; Masumura, R.A. A model for flow stress dependence on grain size for nanocrytallinesolids. *In*: SURYANARAYANA, C.; SINGH, J.; FROES, F.H. *Processing and properties of nanocrystalline materials*. Warrendale: TMS, 1996. p. 387.

[36] HIRTH, J. P.; LOTHE, J. *Theory of dislocations*. 2. ed. Malabar: Krieger Publishing Company, 1982.

[37] MALYGIN, G. A. Breakdown of the Hall–Petch law in micro- and nanocrystalline metals. *Physics of the Solid* State, v. 37, p. 1248, 1995.

[38] SIEGEL, R. W.; FOUGERE, G. E. Mechanical properties of nanophase metals. *Nanostructured Materials*, v. 6, n. 1–4, p. 205–216, 1995.

[39] GRYAZNOV, V. G.; KAPRELOV, A. M.; ROMANOV, A. E. Size effect of dislocation stability in small particles and microcrystallites. *Scripta Metallurgica*, v. 23, n. 8, p. 1443–1448, 1989.

[40] ROMANOV, A. E. Continuum theory of defects in nanoscaled materials. *Nanostructured Materials*, v. 6, n. 1–4, p. 125–134, 1995.

[41] CHOKSHI, A. H. et al. On the validity of the Hall-Petch relationship in nanocrystalline materials. *Scripta Metallurgica,* v. 23, n. 10, p. 1679-1683, 1989.

[42] COBLE, R. L. A model for boundary diffusion controlled creep in polycrystalline materials. *Journal of Applied Physics*, v. 34, n. 6, p. 1679–1682, 1963.

[43] HERRING, C. Diffusional viscosity of a polycrystalline solid. *Journal of Applied Physics*, v. 21, n. 5, p. 437–445, 1950.

[44] KIM, W. J. Explanation for deviations from the Hall-Petch Relation based on the creep behavior of an ultrafine-grained Mg-Li alloy with low diffusivity. *Scripta Materialia*, v. 61, n. 6, p. 652–655, 2009.

[45] KIM, W. J. On Coble creep in Mg-9Al-1Zn alloy with ultrafine-grained microstructure. Scripta Materialia, v. 58, n. 8, p. 659–662, 2008.

[46] LEE, T. J.; PARK, Y. B.; KIM, W. J. Importance of diffusional creep in fine grained Mg-3Al-1Zn alloys. Materials Science and Engineering A, v. 580, p. 133–141, 2013.

[47] MASUMURA, R. A.; HAZZLEDINE, P. M.; PANDE, C. S. Yield stress of fine grained materials. *Acta Materialia*, v. 46, n. 13, p. 4527–4534, 1998.

[48] PANDE, C. S.; COOPER, K. P. Nanomechanics of Hall-Petch relationship in nanocrystalline materials. *Progress in Materials Science*, v. 54, n. 6, p. 689–706, 2009.

[49] NAIK, S. N.; WALLEY, S. M. The Hall–Petch and inverse Hall–Petch relations and the hardness of nanocrystalline metals. *Journal of Materials Science*, v. 55, n. 7, p. 2661–2681, 2020.

[50] KOCH, C. C.; NARAYAN, J. The inverse Hall-Petch effect - Fact or artifact? *Materials Research Society Symposium - Proceedings*, v. 634, p. 1–11, 2001.

[51] GAO, L.; CHEN, R. S.; HAN, E. H. Effects of rare-earth elements Gd and Y on the solid solution strengthening of Mg alloys. *Journal of Alloys and Compounds*, v. 481, n. 1–2, p. 379–384, 2009.

[52] GAO, L.; CHEN, R. S.; HAN, E. H. Microstructure and strengthening mechanisms of a cast Mg-1.48Gd-1.13Y-0. 16Zr (at.%) alloy. *Journal of Materials Science*, v. 44, n. 16, p. 4443–4454, 2009.

[53] MIURA, S. et al. Effect of rare-earth elements Y and Dy on the deformation behavior of Mg alloy single crystals. *Materials Transactions*, v. 49, n. 5, p. 952–956, 2008.

[54] CHEN, K.; BOYLE, K. P. Alloy solid solution strengthening of Mg alloys: Valence effect. *Physica Status Solidi (B) Basic Research*, v. 249, n. 11, p. 2089–2095, 2012.

[55] YASI, J. A.; HECTOR, L. G.; TRINKLE, D. R. First-principles data for solid-solution strengthening of magnesium: From geometry and chemistry to properties. *Acta Materialia*, v. 58, n. 17, p. 5704–5713, 2010.

[56] NIE, J. F. Precipitation and hardening in magnesium alloys. *Metallurgical and Materials Transactions A: Physical Metallurgy and Materials Science*, v. 43, n. 11, p. 3891-3939, 2012.

[57] NATARAJAN, A. R. et al. On the early stages of precipitation in dilute Mg-Nd alloys. *Acta Materialia*, v. 108, p. 367–379, 2016.

[58] MA, L. et al. Texture and mechanical behavior evolution of age-hardenable Mg-Nd-Zn extrusions during aging treatment. *Materials Science and Engineering A*, v. 529, n. 1, p. 151–155, 2011.

[59] XIA, X.; LUO, A. A.; STONE, D. S. Precipitation sequence and kinetics in a Mg-4Sm-1Zn-0.4Zr (wt%) alloy. *Journal of Alloys and Compounds*, v. 649, p. 649–655, 2015.

[60] SANATY-ZADEH, A.; LUO, A. A.; STONE, D. S. Comprehensive study of phase transformation in age-hardening of Mg-3Nd-0.2Zn by means of scanning transmission electron microscopy. *Acta Materialia*, v. 94, p. 294–306, 2015.

[61] BOHLEN, J. et al. Effect of rare earth elements on the microstructure and texture development in magnesium – manganese alloys during extrusion. *Materials Science & Engineering A*, v. 527, n. 26, p. 7092–7098, 2010.

[62] BOHLEN, J. et al. Influence of the alloying additions on the microstructure development of extruded Mg-Mn alloys. In: PROCEEDINGS OF THE MINERALS, METALS & MATERIALS SOCIETY – TMS, 2009. 10. San Francisco. *Magnesium Technology 2009*... Hoboken: Wiley, 2009. p. 225–230.

[63] MOSTAFA, A. et al. The Mg-Mn-Nd system: experimental investigation coupled with thermodynamic modelling. In: INTERNATIONAL CONFERENCE ON MAGNESIUM ALLOYS AND THEIR APPLICATIONS, 2012. 9. Vancouver. *Proceedings*... 2012. p. 245-250.

[64] OKAMOTO, H. Mg-Nd. *Journal of Phase Equilibria and Diffusion*, v. 28, n. 4, 2007.

[65] LEFEBVRE, W.; KOPP, V.; PAREIGE, C. Nano-precipitates made of atomic pillars revealed by single atom detection in a Mg-Nd alloy. *Applied Physics Letters*, v. 100, n. 14, 2012.

[66] SAITO, K.; HIRAGA, K. The structures of precipitates in an Mg-0.5at%Nd age-hardened alloy studied by HAADF-STEM technique. *Materials Transactions*, v. 52, n. 10, p. 1860–1867, 2011.

[67] CHOUDHURI, D. et al. Homogeneous and heterogeneous precipitation mechanisms in a binary Mg-Nd alloy. Journal of Materials Science, v. 49, n. 20, p. 6986–7003, 2014.

[68] SOLOMON, E. L. S.; MARQUIS, E. A. Deformation behavior of β′ and β‴ precipitates in Mg-RE alloys. Materials Letters, v. 216, p. 67 - 69, 2018.

[69] OKAMOTO, H. Supplemental literature review of binary phase diagrams: B-La, B-Zn, Bi-La, Bi-Ti, Cd-Pr, Ce-Ga, Cu-Na, Ge-Ta, Ge-Y, H-Zr, Na-Si, and Pb-Sc. *Journal of Phase Equilibria and Diffusion*, v. 36, n. 6, p. 644–655, 2015.

[70] ROBINSON, H. A.; GEORGE, P. F. Effect of alloying and impurity elements in magnesium alloy cast anodes. *Corrosion*, v. 10, n. 6, p. 182 - 188, 1954.

[71] CELIKIN, M.; KAYA, A. A.; PEKGULERYUZ, M. Effect of manganese on the creep behavior of magnesium and the role of α-Mn precipitation during creep. *Materials Science and Engineering A*, v. 534, p. 129–141, 2012.

[72] HOMMA, T. et al. Effect of Mn addition on creep property in Mg-2Al-2Ca systems. In: PROCEEDINGS OF THE MINERALS, METALS & MATERIALS SOCIETY – TMS, 2011. 12. San Diego. *Magnesium Technology 2011...* Pittsburgh: TMS, 2011. p. 223–226.

[73] ROBSON, J. D.; HENRY, D. T.; DAVIS, B. Particle effects on recrystallization in magnesium-manganese alloys: particle pinning. *Materials Science and Engineering A*, v. 528, n. 12, p. 4239–4247, 2011.

[74] HIDALGO-MANRIQUE, P. et al. Effect of Nd additions on extrusion texture development and on slip activity in a Mg-Mn alloy. *Metallurgical and Materials Transactions A: Physical Metallurgy and Materials Science*, v. 44, n. 10, p. 4819–4829, 2013.

[75] SMITH, C. S. Introduction to grains, phases, and interfaces: an interpretation of microstructure. *Transactions of the Metallurgical Society of AIME*, v. 175, p. 15-51, 1948.

[76] HULL, D.; BACON, D. J. *Introduction to dislocations*. 4. ed. Oxford: Butterworth-Heinemann, 2001.

[77] COURTNEY, T. H. Mechanical behavior of materials. 2. ed. Long Grove: Waveland Press, 2005.

[78] GOTTSTEIN, G. *Physical foundations of materials science*. 1. ed. Berlin: Springer-Verlag, 2004.

[79] DIETER, G. E. *Mechanical metallurgy*. 1. ed. Singapore: McGraw-Hill, 1988.

[80] MARTIN, J. W. *Precipitation hardening*. 2. ed. Oxford: Butterworth-Heinemann, 1998.

[81] HIRSCH, P.B.; HUMPHREYS, F. J. Plastic deformation of two-phase alloys containing small nondeformable particle. *In*: ARCON, A. S.; OROWAN, E. *Physics of strength and plasticity*. 1. ed. Cambridge: MIT Press, 1969, p.189-216.

[82] SMALLMAN, R. E.; NGAN, A. H. W. *Modern physical metallurgy*. 8. ed. Oxford: Butterworth-Heinemann, 2013.

[83] WANG, J.; STANFORD, N. Investigation of precipitate hardening of slip and twinning in Mg5%Zn by micropillar compression. *Acta Materialia*, v. 100, p. 53–63, 2015.

[84] NIE, J. F. Effects of precipitate shape and orientation on dispersion strengthening in magnesium alloys. *Scripta Materialia*, v. 48, n. 8, p. 1009–1015, 2003.

[85] ROBSON, J. D.; STANFORD, N.; BARNETT, M. R. Effect of precipitate shape on slip and twinning in magnesium alloys. *Acta Materialia*, v. 59, n. 5, p. 1945–1956, 2011.

[86] WANG, F.; BHATTACHARYYA, J. J.; AGNEW, S. R. Effect of precipitate shape and orientation on Orowan strengthening of non-basal slip modes in hexagonal crystals, application to magnesium alloys. *Materials Science and Engineering A*, v. 666, p. 114–122, 2016.

[87] HIDALGO-MANRIQUE, P.; ROBSON, J. D.; PÉREZ-PRADO, M. T. Precipitation strengthening and reversed yield stress asymmetry in Mg alloys containing rare-earth elements: a quantitative study. *Acta Materialia*, v. 124, p. 456–467, 2017.

[88] CEPEDA-JIMÉNEZ, C. M.; CASTILLO-RODRÍGUEZ, M.; PÉREZ-PRADO, M. T. Origin of the low precipitation hardening in magnesium alloys. *Acta Materialia*, v. 165, p. 164–176, 2019.

[89] BHATTACHARYYA, J. J. et al. Slip mode dependency of dislocation shearing and looping of precipitates in Mg alloy WE43. *Acta Materialia*, v. 146, p. 55–62, 2018.

[90] ALIZADEH, R.; LLORCA, J. Interactions between basal dislocations and β1′ precipitates in Mg–4Zn alloy: Mechanisms and strengthening. *Acta Materialia*, v. 186, p. 475–486, 2020.

[91] JIANG, J. et al. ⟨c + a⟩ dislocations shearing (0001)α plate precipitates in an Mg-Zn-Mn alloy. *Scripta Materialia*, v. 170, p. 24–28, 2019.

[92] WANG, C. Y.; CEPEDA-JIMÉNEZ, C. M.; PÉREZ-PRADO, M. T. Dislocation-particle interactions in magnesium alloys. *Acta Materialia*, v. 194, p. 190–206, 2020.

[93] VALIEV, R. Z.; ISLAMGALIEV, R. K.; ALEXANDROV, I. V. Bulk nanostructured materials from severe plastic deformations. *Progress in Materials Science*, v. 45, p. 103-189, 2000.

[94] KWAK, E. J. et al. Processing and mechanical properties of fine grained magnesium by equal channel angular pressing. *Materials Transactions*, v. 49, n. 5, p. 1006–1010, 2008.

[95] CETLIN, P. R. et al. Avoiding cracks and inhomogeneities in billets processed by ECAP. *Journal of Materials Science*, v. 45, n. 17, p. 4561–4570, 2010.

[96] FIGUEIREDO, R. B.; CETLIN, P. R.; LANGDON, T. G. Stable and unstable flow in materials processed by equal-channel angular pressing with an emphasis on magnesium alloys. *Metallurgical and Materials Transactions A: Physical Metallurgy and Materials Science*, v. 41, n. 4, p. 778–786, 2010.

[97] HUANG, Y. et al. Evolution of strength and homogeneity in a magnesium AZ31 alloy processed by high-pressure torsion at different temperatures. *Advanced Engineering Materials*, v. 14, n. 11, p. 1018–1026, 2012.

[98] ALSUBAIE, S. A. et al. Evolution of microstructure and hardness in an AZ80 magnesium alloy processed by high-pressure torsion. *Journal of Materials Research and Technology*, v. 5, n. 2, p. 152–158, 2016.

[99] AL-ZUBAYDI, A. et al. Structural and hardness inhomogeneities in Mg-Al-Zn alloys processed by high-pressure torsion. *Journal of Materials Science*, v. 48, n. 13, p. 4661–4670, 2013.

[100] ZHILYAEV, A. P. et al. Experimental parameters influencing grain refinement and microstructural evolution during high-pressure torsion. *Acta Materialia*, v. 51, n. 3, p. 753–765, 2003.

[101] WETSCHER, F. et al. Structural refinement of low alloyed steels during severe plastic deformation. *Materials Science and Engineering: A*, v. 387–389, n. 1–2, p. 809–816, 2004.

[102] HARAI, Y. et al. Microstructural and mechanical characteristics of AZ61 magnesium alloy processed by high-pressure torsion. *Materials Transactions*, v. 49, n. 1, p. 76–83, 2008.

[103] JIANG, H. et al. Microstructural evolution, microhardness and thermal stability of HPT-processed Cu. *Materials Science and Engineering: A*, v. 290, n. 1, p. 128–138, 2000.

[104] ZHILYAEV, A. P. et al. Microhardness and microstructural evolution in pure nickel during high-pressure torsion. *Scripta Materialia*, v. 44, p. 2753–2758, 2001.

[105] XU, C.; HORITA, Z.; LANGDON, T. G. The evolution of homogeneity in an aluminum alloy processed using high-pressure torsion. *Acta Materialia*, v. 56, n. 18, p. 5168–5176, 2008.

[106] IVANISENKO, Y.; VALIEV, R. Z.; FECHT, H. J. Grain boundary statistics in nano-structured iron produced by high pressure torsion. *Materials Science and Engineering: A*, v. 390, n. 1–2, p. 159–165, 2005.

[107] ESTRIN, Y. et al. Strain gradient plasticity modelling of high-pressure torsion. *Journal of the Mechanics and Physics of Solids*, v. 56, n. 4, p. 1186–1202, 2008.

[108] MOLOTNIKOV, A. Application of strain gradient plasticity modelling to high pressure torsion. *Materials Science Forum*, v. 584-586, p. 1051–1056, 2008.

[109] MISHRA, A. et al. Microstructural evolution in copper subjected to severe plastic deformation: Experiments and analysis. *Acta Materialia*, v. 55, n. 1, p. 13–28, 2007.

[110] FIGUEIREDO, R. B.; LANGDON, T. G. Processing magnesium and its alloys by high-pressure torsion: an overview. *Advanced Engineering Materials*, v. 1801039, p. 1–15, 2018.

[111] ION, S. E.; HUMPHREYS, F. J.; WHITE, S. H. Dynamic recrystallisation and the development of microstructure during the high temperature deformation of magnesium. *Acta Metallurgica*, v. 30, n. 10, p. 1909–1919, 1982.

[112] GALIYEV, A.; KAIBYSHEV, R.; GOTTSTEIN, G. Correlation of plastic deformation and dynamic recrystallization in magnesium alloy ZK60. *Acta Materialia*, v. 49, n. 7, p. 1199–1207, 2001.

[113] MYSHLYAEV, M. M. et al. Twinning, dynamic recovery and recrystallization in hot worked Mg-Al-Zn alloy. *Materials Science and Engineering: A*, v. 337, n. 1–2, p. 121–133, 2002.

[114] BEER, A. G.; BARNETT, M. R. Influence of initial microstructure on the hot working flow stress of Mg-3Al-1Zn. *Materials Science and Engineering: A*, v. 423, n. 1–2, p. 292–299, 2006.

[115] POGGIALI, F. S. J. et al. Grain refinement of commercial purity magnesium processed by ECAP (Equal Channel Angular Pressing). *Materials Research*, v. 15, n. 2, p. 312–316, 2012.

[116] SERRE, P. et al. Influence of strain rate on the characteristics of a magnesium alloy processed by high-pressure torsion. *Materials Science and Engineering: A*, v. 528, n. 10–11, p. 3601–3608, 2011.

[117] SILVA, C. L. P. et al. Microstructure and hardness evolution in magnesium processed by HPT. *Materials Research*, v. 20, p. 2–7, 2017.

[118] FIGUEIREDO, R. B. et al. Evidence for exceptional low temperature ductility in polycrystalline magnesium processed by severe plastic deformation. *Acta Materialia*, v. 122, p. 322–331, 2017.

[119] CRUMP, J.; QIAO, X. G.; STARINK, M. J. The effect of high-pressure torsion on the behaviour of intermetallic particles present in Al-1Mg and Al-3Mg. *Journal of Materials Science*, v. 47, n. 4, p. 1751–1757, 2012.

[120] SAUVAGE, X.; WETSCHER, F.; PAREIGE, P. Mechanical alloying of Cu and Fe induced by severe plastic deformation of a Cu-Fe composite. *Acta Materialia*, v. 53, n. 7, p. 2127–2135, 2005.

[121] BACHMAIER, A. et al. The formation of supersaturated solid solutions in Fe-Cu alloys deformed by high-pressure torsion. *Acta Materialia*, v. 60, n. 3, p. 860–871, 2012.

[122] MASSALSKI, T. B. et al. *Binary alloy phase diagrams*. 1. ed. Metals Park: American Society for Metals, 1986. p. 915.

[123] YAVARI, A. R.; DESRÉ, P. J.; BENAMEUR, T. Mechanically driven alloying of immiscible elements. *Physical Review Letters*, v. 68, n. 14, p. 2235–2238, 1992.

[124] SALJE, G.; FELLER-KNIEPMEIER, M. The diffusion and solubility of iron in copper. *Journal of Applied Physics*, v. 49, n. 1, p. 229–232, 1978.

[125] MEHRER, H. Diffusion in Solids. Dresden: Springer, 2007. 651 p. (The Springer Series in Solid-State Sciences, v. 155).

[126] STRAUMAL, B. B. et al. Formation of nanograined structure and decomposition of supersaturated solid solution during high pressure torsion of Al-Zn and Al-Mg alloys. *Acta Materialia*, v. 52, n. 15, p. 4469–4478, 2004.

[127] TURNBULL, D.; HOFFMAN, R. E. The effect of relative crystal and boundary orientations on grain boundary diffusion rates. *Acta Metallurgica*, v. 2, n. 3, p. 419–426, 1954.

[128] FUJINAGA, Y.; SATO, T. The aluminum-zinc phase diagram under high pressure. *Journal of Alloys and Compounds*, v. 209, n. 1–2, p. 311–317, 1994.

[129] SOER, W. A.; CHEZAN, A. R.; DE HOSSON, J. T. M. Deformation and reconstruction mechanisms in coarse-grained superplastic Al-Mg alloys. *Acta Materialia*, v. 54, n. 14, p. 3827–3833, 2006.

[130] QI, W. H.; WANG, M. P. Vacancy formation energy of small particles. Journal of Materials Science, v. 39, p. 2529– 2530, 2004.

[131] SATO, K. et al. Point defect production under high internal stress without dislocations in Ni and Cu. *Radiation Effects and Defects in Solids*, v. 157, n. 1–2, p. 171–178, 2002.

[132] SATO, K. et al. Simulation of vacancy migration energy in Cu under high strain. *Materials Science and Engineering: A*, v. 350, n. 1–2, p. 220–222, 2003.

[133] CAHN, R.W.; HASEN, P. *Physical metallurgy*. 3. ed. Amsterdam: North-Holland Physics Publishing; 1983. p. 385.

[134] LEJCEK, P. *Grain boundary segregation in metals*. 1. ed. Berlin: Springer, 2010. 249 p. (The Springer Series in Materials Sciences, v. 136).

[135] VALIEV, R. Z. et al. On the origin of the extremely high strength of ultrafine-grained Al alloys produced by severe plastic deformation. *Scripta Materialia*, v. 63, n. 9, p. 949–952, 2010.

[136] SAUVAGE, X. et al. Grain boundary segregation in UFG alloys processed by severe plastic deformation. *Advanced Engineering Materials*, v. 14, n. 11, p. 968–974, 2012.

[137] VO, N. Q. et al. Reaching theoretical strengths in nanocrystalline Cu by grain boundary doping. *Scripta Materialia*, v. 65, n. 8, p. 660–663, 2011.

[138] ZHANG, X. F. et al. Influences of grain size and grain boundary segregation on mechanical behavior of nanocrystalline Ni. *Materials Science and Engineering: A*, v. 527, n. 9, p. 2297–2304, 2010.

[139] SUN, W. T. et al. Altered ageing behaviour of a nanostructured Mg-8.2Gd-3.8Y-1.0Zn-0.4Zr alloy processed by high pressure torsion. *Acta Materialia*, v. 151, p. 260–270, 2018.

[140] SUN, W. T. et al. Achieving ultra-high hardness of nanostructured Mg-8.2Gd-3.2Y-1.0Zn-0.4Zr alloy produced by a combination of high pressure torsion and ageing treatment. *Scripta Materialia*, 2018.

[141] HEGEDUS, Z. et al. The effect of impurity level on ultrafine-grained microstructures and their stability in low stacking fault energy silver. *Materials Science and Engineering; A*, v. 528, n. 29–30, p. 8694–8699, 2011.

[142] ZHANG, H. W. et al. Thermal behavior of Ni (99.967% and 99.5% purity) deformed to an ultra-high strain by high pressure torsion. *Acta Materialia*, v. 58, n. 5, p. 1698–1707, 2010.

[143] SCHÄFER, J.; STUKOWSKI, A.; ALBE, K. Plastic deformation of nanocrystalline Pd-Au alloys: On the interplay of grain boundary solute segregation, fault energies and grain size. *Acta Materialia*, v. 59, n. 8, p. 2957–2968, 2011.

[144] ANTHONY, T. R. Solute segregation in vacancy gradients generated by sintering and temperature changes. *Acta Metallurgica*, v. 17, n. 5, p. 603–609, 1969.

[145] HONDROS, E. D. Ségrégations intergranulaires - Grain boundary segregation the current situation and future requirements. *Journal de Physique Colloques*, v. 36, n. C4, p. 117–135, 1975.

[146] SAUVAGE, X. et al. Atomic-scale analysis of the segregation and precipitation mechanisms in a severely deformed Al-Mg alloy. *Acta Materialia*, v. 72, p. 125–136, 2014.

[147] ROBSON, J. D. et al. Grain boundary segregation of rare-earth elements in magnesium alloys. *Metallurgical and Materials Transactions A: Physical Metallurgy and Materials Science*, v. 47, n. 1, p. 522–530, 2016.

[148] HORKY, J. et al. Exceptional strengthening of biodegradable Mg-Zn-Ca alloys through high pressure torsion and subsequent heat treatment. *Materials*, v. 12, n. 15, 2019.

[149] BASHA, D. A. et al. Interfacial segregation induced by severe plastic deformation in a Mg–Zn–Y alloy. *Scripta Materialia*, v. 124, p. 169–173, 2016.

[150] BASHA, D. A. et al. Effect of processing strain rate and temperature on interfacial segregation of zinc in a magnesium alloy. *Materials Science and Engineering: A*, v. 703, n. April, p. 54–67, 2017.

[151] ROBSON, J. D. Effect of rare-earth additions on the texture of wrought magnesium alloys: The role of grain boundary segregation. *Metallurgical and Materials Transactions A: Physical Metallurgy and Materials Science*, v. 45, n. 8, p. 3205–3212, 2014.

[152] MCLEAN, D. Grain Boundaries in Metals. Oxford: Clarendon Press, 1957. 345 p.

[153] BOUREZQ, Y. I. et al. Texture and microhardness of Mg-Rare Earth (Nd and Ce) alloys processed by high-pressure torsion. *Materials Science & Engineering: A*, 2018.

[154] QIAO, X. G. et al. Hardening mechanism of commercially pure Mg processed by high pressure torsion at room temperature. *Materials Science and Engineering: A*, v. 619, p. 95–106, 2014.

[155] ČÍŽEK, J. et al. Defects in ultra-fine grained Mg and Mg-based alloys prepared by high pressure torsion studied by positron annihilation. *Acta Physica Polonica A*, v. 107, n. 5, p. 738–744, 2016.

[156] XU, J. et al. Microhardness, microstructure and tensile behavior of an AZ31 magnesium alloy processed by high-pressure torsion. *Journal of Materials Science*, v. 50, n. 22, p. 7424–7436, 2015.

[157] BRYŁA, K. et al. Effect of high-pressure torsion on grain refinement, strength enhancement and uniform ductility of EZ magnesium alloy. *Materials Letters*, v. 212, p. 323–326, 2018.

[158] PENNYCOOK, S. J. et al. Scanning transmission electron microscopy for nanostructure characterization. *In*: ZHOU, W.; WANG, Z. L. (Ed.) *Scanning Microscopy for Nanotechnology.* New York: Springer, 2007. p. 152-191.

[159] PETROVA, R. V. Quantitative high-angle annular dark field scanning transmission electron microscopy for materials science. 2006. Dissertation (Doctor of Philosophy in Physics) - College of Sciences, University of Central Florida, Orlando.

4 Development of segregations in a Mg-Mn-Nd alloy during HPT processing

Paula Campos de Oliveira[1], Luciano A. Montoro[2], Maria Teresa Perez-Prado[3], Anton Hohenwarter[4], Roberto B. Figueiredo[1,*], Augusta Isaac[1]

[1] Department of Metallurgical and Materials Engineering, Universidade Federal de Minas Gerais, Belo Horizonte, MG 31270-901, Brazil.

[2] Department of Chemistry, Universidade Federal de Minas Gerais, Belo Horizonte, MG 31270-901, Brazil.

[3] IMDEA Materials Institute, Madrid, 28906, Spain

[4] Department of Materials Science, Chair of Materials Physics, Montanuniversität Leoben, Jahnstraße 12, 8700 Leoben, Austria

Abstract:

The present work evaluates the segregation of alloying elements during severe plastic deformation of a magnesium alloy. A Mg-1wt% Mn-1wt% Nd alloy was processed by high-pressure torsion and the microstructure was characterized by X-ray diffraction, scanning and transmission electron microscopy. High angular annular dark field images were used to distinguish areas with segregated alloying elements. The results show that Nd readily segregates along boundaries in the early stage of deformation while Mn, which was dispersed as small particles in the starting material, undergoes slow fragmentation forming nanoparticles distributed throughout the microstructure and segregates along boundaries. The evolution of microhardness shows a rapid increase in strength at low imposed strains and saturates. It is suggested that Mn plays only a minor role on the contribution to the strength of this alloy, because the slow development of nano-clusters and segregations of this element is not accompanied by changes in hardness.

Keywords: segregation; magnesium alloy; severe plastic deformation; high-pressure torsion

1. Introduction

It is now well known that severe plastic deformation by high-pressure torsion can induce the formation of supersaturated solid solutions [1, 2] and segregations [3, 4] of alloying elements along grain boundaries. It is also possible to mix different phases and obtain metastable materials with superior properties [5]. The mechanisms responsible for these observations have been studied and, although they are not yet clear, some evidences have been established. For example, it is known that deformation during HPT is not always limited to the shear plane. Folding of phases and formation of vortices have been reported [6]. These instabilities increase locally the amount of deformation and contribute to mechanical mixing. Also, the severe plastic deformation is associated with the formation of a high density of defects in the crystalline structure that can contribute to enhanced diffusion and mixing on an atomic level.

Segregations in different magnesium alloys processed by HPT have been reported in recent years. Atom probe tomography showed segregations of Zn and Ca in a Mg-Zn-Ca alloy processed by HPT [7]. Earlier papers had also identified segregations of Zn along grain boundaries using high angular annular dark field (HAADF) images and EDS mapping in TEM [8-10]. Similar techniques (HAADF and EDS mapping) showed evidence of segregations of Gd, Y and Zn in a magnesium alloy [11, 12]. These segregations are usually associated with higher hardness and thermal stability which increases the interest in understanding their formation.

It has been shown that Mg-Mn-RE alloys develop weak textures in extrusion and this is associated with improved ductility and reduced yield asymmetry in tension and compression. Among the rare-earth (RE) elements, it appears that Nd is the most effective element to achieve this goal [13]. It has been recently reported that Nd containing prismatic plates increase the critical resolved shear stress (CRSS) for basal slip moderately, as basal dislocations are able to shear them both in the transverse and longitudinal directions [14-17]. Still, an increase in hardness attributed to precipitation

has been reported in a Mg-1.43%Nd alloy processed by high pressure torsion (HPT) [18]. Manganese is also an important alloying element for magnesium due to its ability to scavenge Fe which is a detrimental element for corrosion [19]. Moreover, manganese does not form intermetallics with Mg. The Mg-1wt% Mn-1wt% Nd (MN11) alloy is, therefore, an interesting alloy to investigate the formation of segregations during HPT as it contains one element, Nd, with a high propensity to form intermetallics and one, Mn, which does not develop such compounds.

The aim of this work is to investigate the microstructrural evolution in a MN11 alloy following processing by HPT to different strain levels. In particular, the distribution of phases and the segregation of elements to grain boundaries have been examined using high resolution transmission electron microscopy.

2. Materials and Methods

The material used in the present investigation was a Mg-1%wt. Mn-1%wt. Nd (MN11) alloy. Billets of this material were first produced by gravity casting, homogenized at 350ºC for 15 h, and then machined up to a diameter of 93 mm for extrusion. Indirect extrusion was carried out at 300 ºC and 5.5 mm/s to produce round bars of 17 mm in diameter, which corresponds to an extrusion ratio of 1:30. The resulting microstructure is termed throughout the entire text the “as-extruded” condition. The average grain size, determined using the mean linear intercept method, was ~15 μm. Disks with a diameter of 8.0 mm and 1.0 mm in thickness were machined out of the extruded bars and processed by HPT at room temperature using a quasi-constrained facility. The nominal pressure during processing was 6 GPa. Some samples were subjected to pressure without rotation and are referred to as N = 0. Other samples were subjected to torsion under pressure to 1/4, 1, 2 and 5 turns. The final thickness of the samples was ~0.8 mm.

The phases present in the samples were examined by x-ray diffraction (XRD). The equipment used was a Philips PW1710 diffractometer with Cu Kα radiation and a graphite

monochromatic crystal with a wavelength of 1.5406 Å. The step size was 0.020° and the time per step was 1 s. Discs were polished to a mirror-like finishing and the microstructure was observed using a Quanta FEG 3D FEI microscope equipped with energy-dispersive x-ray spectroscopy (EDS). Electron transparent lamellas were extracted from the mid-radius by focused ion beam (FIB) using the same equipment.

The lamellae were investigated by transmission electron microscopy (TEM) using a FEI Titan Themis Cubed (FEI Company) microscope, equipped with a Cs probe corrector and a Super-X EDS with four windowless silicon-drift detectors and operated at 300 kV. Images were collected using scanning transmission electron microscopy (STEM) technique. Bright field (BF) and high angular annular dark field (HAADF) images were recorded. The HAADF technique provides the ability to differentiate elements with different atomic weight and has been used to investigate the formation of precipitates in Mg-Nd alloys [20, 21].

Microhardness measurements were performed within one-quarter of the disks and across their diameters, with 0.5 mm separation between the indentations. Microhardness tests were carried at load force of 100 gf and a dwell time of 10 s in a Future-Tech FM-700 tester equipped with a Vickers diamond indenter.

3. Results

3.1. General microstructure

Figure 4.1 shows the XRD patterns obtained for the samples in the as-extruded condition, after application of pressure without rotation (N = 0) and after different levels of rotation (N = ¼,1,2,5). The peak distribution remains relatively unchanged after processing to high strains. The main peaks belong to the Mg solid solution and minor peaks associated with Mn are also present. Additionally, several small peaks, corresponding to Mg-Nd intermetallics, are also apparent. Out of those several could be the attributed to the Mg_3Nd intermetallic phase, while others have not been identified.

These likely correspond to other Mg-Nd metastable precipitates, whose composition has, to date, not been clearly established. Indeed, the sequence of precipitation from the supersaturated solid solution state in Mg-Nd alloys has long been under debate and it remains partially unknown [20, 22, 23]. The Mg_3Nd phase has been reported in different experiments [20, 21, 24] including a Mg-1.43% Nd alloy processed by HPT [25, 26].

Figure 4.2 shows the surface of the different samples observed using a backscattered electron signal in an SEM. Bright spots are clearly distinguished in all samples although their size appears larger in the as-extruded condition. Bright areas indicate the presence of elements with higher atomic number, and therefore, in the current alloy, correspond to a higher concentration of Mn and/or Nd. Higher magnification images of these bright phases are depicted as inserts and the EDS composition for each of them is given. Even though the composition provided by EDS is not completely accurate due to the influence of the surrounding Mg matrix, the results are fairly consistent with a Mg_3Nd phase. This supports the assumption that this phase is present in the alloy before and after HPT processing. Metallic manganese as an additional phase was not observed using SEM.

STEM BF images of samples processed to 1, 2 and 5 turns are presented in Fig. 4.3. It is noticed that the grain structure was significantly refined after only one turn of HPT. The (sub)grain sizes, determined as the average of the mean diameter of individual (sub)grains, were 240 nm, 220 nm and 200 nm for samples processed to 1, 2 and 5 turns, respectively. These (sub)grain sizes are smaller than that reported for a Mg-1.43% Nd alloy processed to 5 turns of HPT [18], which amounted to 650 nm. This difference in grain size is attributed to the different techniques used to evaluate the grain structure as STEM images were used in the present investigation and EBSD was used elsewhere [18]. Thus, while all boundaries were considered in the present investigation, the EBSD analysis [18] only considered grains with appropriate confidence index, with a minimum of 5 pixels (each pixel being 50 nm) and separated by boundaries with misorientations larger than 5^o. Also, the material used in the present investigation contains Mn, which might enhance the grain refinement ability of the material. Dark spots in the range of tens

of nanometers were observed in the BF images in all samples including the extruded material and it is apparent that their size decreases with increasing the number of turns imposed during HPT. Figure 4.4 shows HAADF images of the as-extruded sample and the sample processed to 5 turns of HPT and several bright particles in the range of tens of microns are readily observed in both of them. Bright areas in this image also indicates the presence of elements with higher atomic number which can be Mn and/or Nd in the present alloy. HPT causes a decrease in average size of these particles but does not change their aspect ratio. These spots are attributed to metallic Mn. Multiple EDS composition maps were acquired in regions near these spots and they show a high concentration of Mn. Figure 4.5 shows one of these maps taken from the extruded sample. The out of plane dimension of the Mn phase is smaller than the thickness of the lamella and therefore it is expected that the Mg matrix surrounds this phase. This would explain the homogeneous distribution of Mg in the element map. It is also apparent that the amount of Nd in solid solution in the extruded alloy is higher than Mn.

3.2 Segregation of alloying elements

Careful observation of the microstructure of the HPT processed samples using HAADF images and EDS mapping allowed to distinguish grain boundary segregations of Mn and Nd. Figure 4.6 shows a HAADF image of the sample processed to 1 turn of HPT in which a bright particle is present in the left side and a bright continuous thin line of hundreds of nanometers in length is highlighted using small red arrows. The bright particle on the left is a Mn-rich particle. A higher magnification image of the thin bright line shows evidence of a discontinuity in it, which is pinpointed using a yellow arrow. It is apparent that this line separates grains and that the rotation of one of the neighboring crystallites gave rise to the observed discontinuity. EDS mapping of a small region surrounding the line (dotted red box) reveals clearly the co-segregation of Mn and Nd, as well as segregations of Nd along other boundaries. Overall, while Mn appears to segregate only to selected boundaries, Nd atoms seem to populate the entire grain boundary network.

Figure 4.7 shows a HAADF image of a triple junction in the sample processed to 2 turns. Segregation of alloying elements along the grain boundaries is also clearly noticeable here, as these areas exhibit a much brighter contrast than the dark grain interiors. EDS mapping shows the segregations are mostly related to Nd but spots with a high concentration of Mn are also observed along the grain boundaries.

With increasing number of turns (N=5) segregation of both Nd and Mn is observed along grain boundaries (Fig. 4.8). Additionally, bright spots, corresponding to nanoclusters, are also apparent at the grain interiors. Figure 4.8(a) illustrates several nanocrystalline (sub)grains, with size smaller than 100 nm, whose boundaries are populated with Nd and Mn atoms, as confirmed by the corresponding EDS maps. Higher magnification images were acquired from the areas depicted in Fig. 4.8(a) and they are shown in Figs. 4.8(b-d). Figure 4.8(b) shows on the top a grain boundary, populated with Nd and Mn atoms, as well as some round-shaped brighter areas of a few nanometers in thickness at the bottom. The corresponding EDS maps evidence that the latter are rich in Mn. This suggests that the small bright spots dispersed along grain interiors in Fig. 4.8(a) are nanosized Mn clusters or precipitates. A fast Fourier transform (FFT) analysis of the atomic planar distances revealed, indeed, the presence of crystalline Mn in this area. Figure 4.8(c) shows a grain boundary in which segregation of heavier elements is clearly also distinguished. Additionally, many nanosized bright spots are clearly observed in this region as well. The FFT of this image reveals the presence of atomic planes separated by 2.6 Å in the grain at the top. This interplanar distance corresponds to Mg (002) planes. The grain at the bottom displays a 2.45 Å interplanar spacing, which is attributed to Mg (101) planes. Additionally, an interplanar spacing of 2.23 Å was measured in the area surrounding one of the bright spots, and this is attributed to the Mn (220) planes. Figure 8(d) shows a boundary with misorientation of only 2º on Mg (102) planes. Segregation of Nd and, to a smaller extent, of Mn, and a discrete Mn-rich region, are observed along the boundary. This further supports the fact that Nd tends to segregate along a large fraction of the boundary network while Mn tends to form nanometer-sized particles and to segregate only to selected boundaries or boundary regions. The observed segregation along such a low angle boundary disagrees with the reported negligible segregations of Cr in nanostructured Fe in low angle boundaries [27].

3.3 Hardness

The distribution of hardness throughout the surface of the as-extruded and HPT processed samples is shown in Fig. 4.9. The as-extruded alloy displays a homogeneous distribution of hardness with values in the range of 45 to 50 Hv. Imposing pressure without rotation leads to an increase of the hardness to values ranging from 60 to 75 HV, and this is attributed to the compressive deformation that takes place in quasi constrained systems. The torsional deformation leads to an additional increase of the hardness, but the values tend to level off after only 1/4 of a turn.

In order to evaluate the strain hardening characteristics of this material, the hardness is also plotted as a function of the effective strain, ε, in Fig. 4.10. The latter was calculated as $\varepsilon = 2\pi Nr/\sqrt{3}h$, where N is the number of turns, r is the distance from the center and h is the thickness of the sample [28, 29]. The average hardness values corresponding to the as-extruded material and to the sample processed by imposing pressure without rotation are also plotted. The strain-hardening is pronounced at low strain levels but tends to saturate at 75 ~ 80 Hv at strains larger than ~10.

4. Discussion

The microstructure of the as-extruded alloy is formed by a magnesium matrix, a supersaturated solid solution of Nd, and by a dispersion of Mn particles that are tens of nanometers in size, as well as by Mg-Nd intermetallic particles. This microstructure changed significantly after processing by HPT.

First, our results evidence that there is a decrease in the average size and in the amount of Mg-Nd intermetallics, as well as segregation of Nd atoms to grain boundaries from the early stages of HPT deformation (N=1). It has been reported that the Mg-Nd

precipitates are easily sheared by basal and pyramidal dislocations at room temperature [17] due to the large geometric compatibility of the Mg lattice with that of the most common precipitates [16]. This is consistent with the observed severe shearing and break up of such precipitates during severe plastic deformation by HPT. It is expected that the Nd atoms resulting from the decomposition of Mg-Nd intermetallics contribute to further supersaturate the Mg solid solution. Segregation of Nd to grain boundaries is attributed to dislocation dragging of solute elements to grain boundaries and/or solute dragging by moving grain boundaries. A recent review [30] on strain induced segregations describes this mechanism and shows experimental evidence of similar segregations in other metallic systems.

It is interesting to note that segregation of Nd was observed along a boundary with only 2º of misorientation which disagrees from the reported reduced segregation of Cr along low angle boundaries in nanocrystalline Fe produced by magnetron sputtering [27]. Such low angle boundary is not expected to act as a sink to dislocations. Therefore its formation cannot be attributed to dislocation drag of solute elements. The grain boundaries are expected to move during severe plastic deformation and this mobility preserves the grain aspect ratio at a low value. Thus, it is possible that a grain boundary can detach from the segregations of alloying elements. This mechanism is similar to the one observed at high stresses in viscous glide creep. In this creep mechanism, moving dislocations drag solute atoms but a breakaway from the solute atmosphere is observed at high stresses. Similarly, it is expected that grain boundary migration can drag solute elements, leading to the formation of segregations, and might detach from this solute segregations at large stresses. This would leave a surface of alloying element segregations inside the grain. Such surface can act as an obstacle to moving dislocations and develop a low angle boundary with the accumulation of some dislocations. It is also known that materials processed by SPD display a higher diffusivity due to the higher dislocaiton density and non-equilibrium state of grain boundaries. This higher diffusivity can facilitate the development of segregations along grain boundaries.

Second, HPT leads to a decrease in average size of Mn particles and promote, at high strains (N=5), a homogeneous distribution of nanosized Mn clusters, dispersed throughout grain interiors (Fig. 4.7). Additionally, Mn atoms segregate to grain boundaries. However, despite the fact that the fraction of Mn atoms in the alloy is significantly higher than the fraction of Nd atoms, the concentration of the former at grain boundaries is smaller than the concentration of the latter at all strains investigated. These observations could be rationalized in the following way. On the one hand, earlier studies have demonstrated that shearing of Mn-rich particles by basal and pyramidal dislocations is rarely observed during room temperature uniaxial testing to strains smaller than 15% due to the smaller geometric compatibility between the Mg matrix and such particles [16]. Consequently, the Mn phases may act as hard particles and will not undergo significant deformation. It has been shown that the mixing effectiveness decreases in situations where there is a large difference in hardness between the phases and the volume fraction of the hard phase is smaller [31]. Moreover, the amount of Mn in solid solution in the Mg matrix is initially lower than that of Nd, as Mn is found mostly in the form of precipitates. Thus, it is our contention that, even though severe straining by HPT leads to a decrease in size of the Mn-rich particles, and to the formation of nanosized clusters, the amount of atoms in solid solution, that are prone to segregation, is still limited. Thus, after 1 turn of HPT, Mn segregation to grain boundaries is only observed along a few discrete “lines” (Fig. 4.6). The lack of Mn in boundaries inclined to these layers confirms that grain boundary diffusion was not the major driving force to trigger dissolution of this element into the matrix. A small discontinuity in a line with Mn segregation in the sample processed to 1 turn of HPT suggests that grain boundary sliding and plastic deformation contributes to breaking up the Mn-rich layers.

Our results show, furthermore, that the hardness increases with low applied deformation and that it saturates after only 1/4 turn of HPT. The saturation hardness observed in the present experiments, ~80 Hv, is higher than observed in pure magnesium (35 ~ 55 Hv) [32-34], confirming the contribution of the alloying elements contribute to the strength of the alloy. Our microstructure analysis revealed that Nd segregates along boundaries after only 1 turn of HPT. No significant change in the distribution of Nd was observed with further processing. Moreover, (sub)grain refinement appears to take place

before 1 turn of HPT and further processing does not change the average (sub)grain size significantly. Therefore, both, the Nd distribution and the (sub)grain refinement, agree with the saturation in hardness observed after only 1 turn. On the other hand, the distribution of Mn changes significantly after several HPT turns. As stated above, while limited segregation of Mn is observed after 1 turn, further straining leads to the formation of Mn nanoparticles and to a wider distribution of Mn atoms along grain boundaries. The lack of change in hardness associated with these microstructural changes suggests that Mn plays only minor role on the strength of this alloy. Consistently, the measured hardness saturation value, 80 Hv, is similar to the value of ~79 Hv reported for a Mg-1.43% Nd alloy, with no Mn as alloying element, which was also processed to 5 turns of HPT [18]. Also, it has been shown that fine-grained Mg-Mn alloys display high strain rate sensitivity [35, 36] but reduced strength when compared to pure Mg with similar grain size [35].

5. Summary and conclusions

A Mg-1% Mn-1% Nd (MN11) alloy was processed at room temperature by high pressure torsion using different numbers of turns. This alloy contains Mg-Nd intermetallic plates, that are easily sheared by dislocations, and Mn-rich particles, which are almost impenetrable to such linear defects. The evolution of the microstructure of this alloy during processing was examined using HAADF, HRSTEM and EDS mapping in the TEM. The main conclusions of this study are the following:

1.-(Sub)grain refinement takes place at the first deformation stages, and the (sub)grain size saturates already after 1 HPT turn.

2.-Segregation of Nd to boundaries takes place readily in such a way that substantial segregation levels are apparent after only 1 turn of HPT and they persist with further processing. Nd atoms are observed to segregate to all boundaries, irrespective of their misorientation, and including low angle boundaries. The mechanism of segregation of Nd is associated with dislocation and grain boundary dragging.

3.-HPT processing results in the break-up of Mn-rich particles, in the discrete segregation of Mn to grain boundaries, and in the formation of nanosized Mn clusters throughout the grain interiors. Mn segregation to grain boundaries is distinctly more sluggish than the segregation of Nd atoms.

4.-The hardness of the HPT processed alloy increases significantly after low strains and saturates at ~80 Hv after only 1 turn. This is attributed to a combination of the observed (sub)grain refinement and the Nd re-distribution, while Mn appears to play only a minor role.

Acknowledgments

The authors acknowledge support from CNPq, CAPES and FAPEMIG. MTPP acknowledges funding from the Spanish Ministry of Science and Innovation (project PID2019-111285RB-I00).

Data availability statement

The raw/processed data required to reproduce these findings cannot be shared at this time due to technical or time limitations.

Figures:

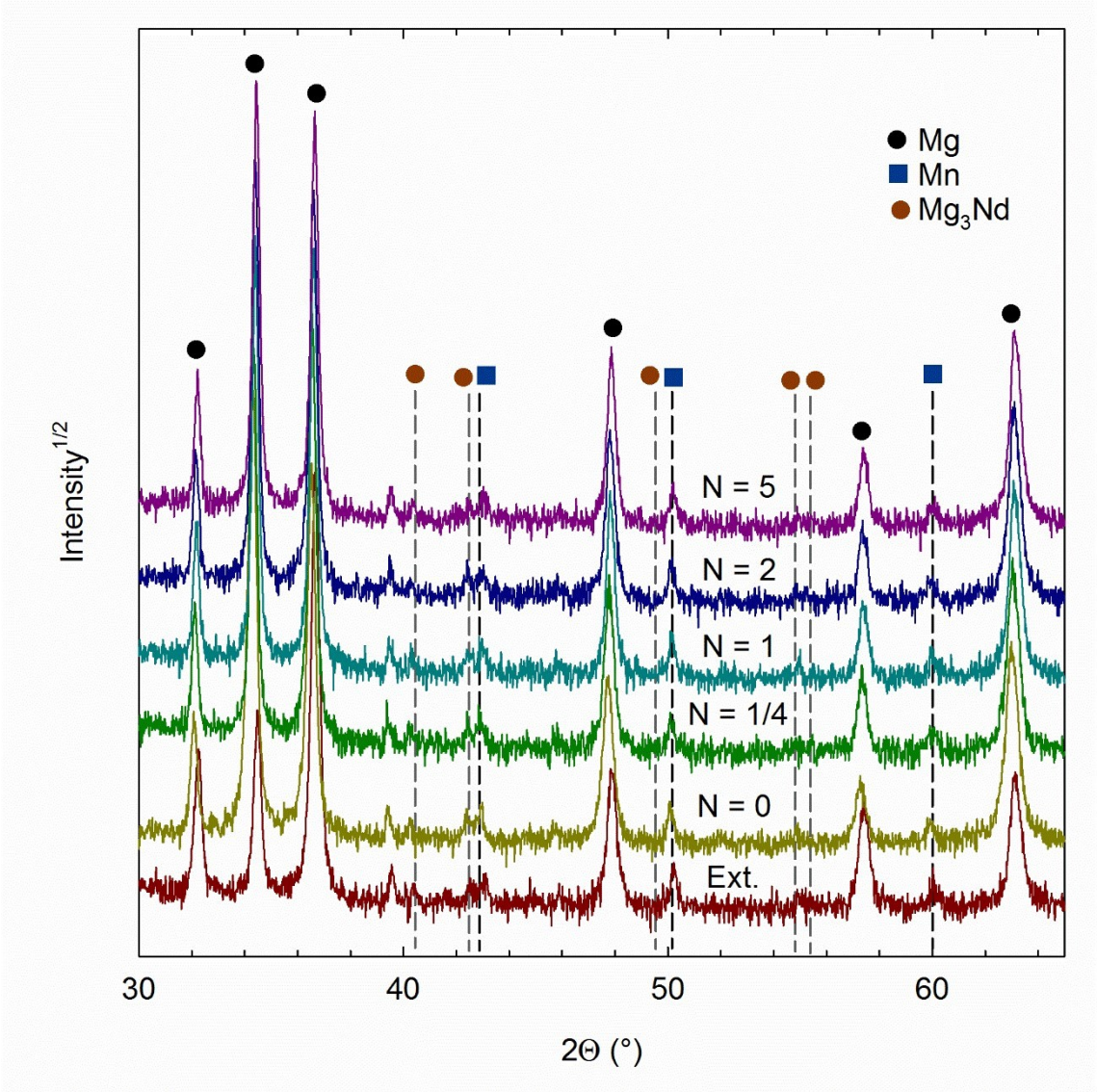

Figure 4.1 - XRD patterns of the as-extruded (ext.) and HPT-processed samples with different number of turns.

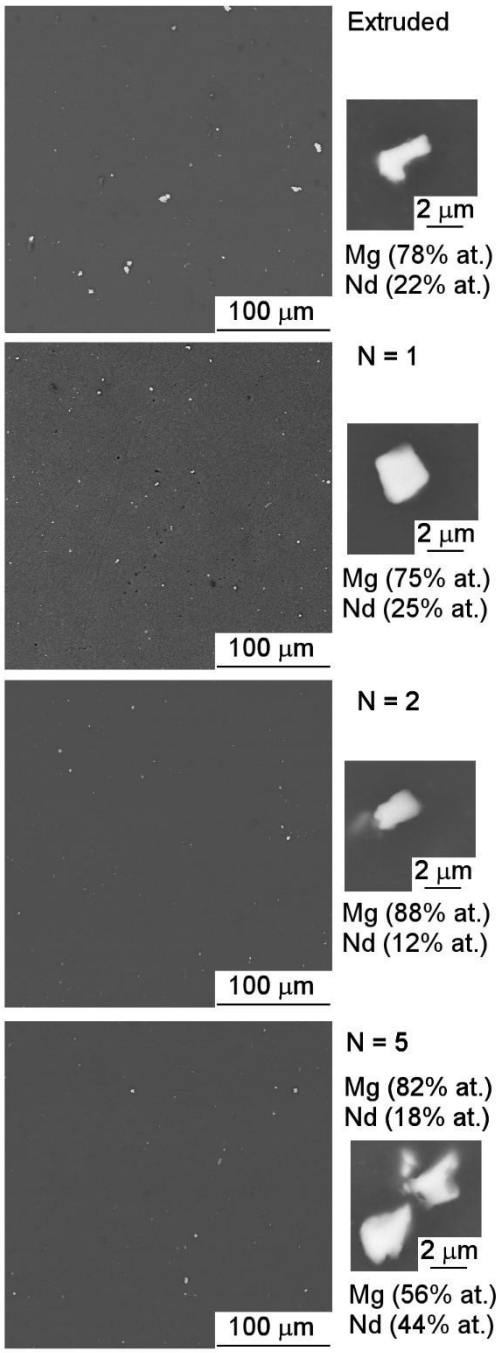

Figure 4.2 - SEM images and EDS analysis of the as-extruded and HPT-processed (N = 1, 2, 5) samples.

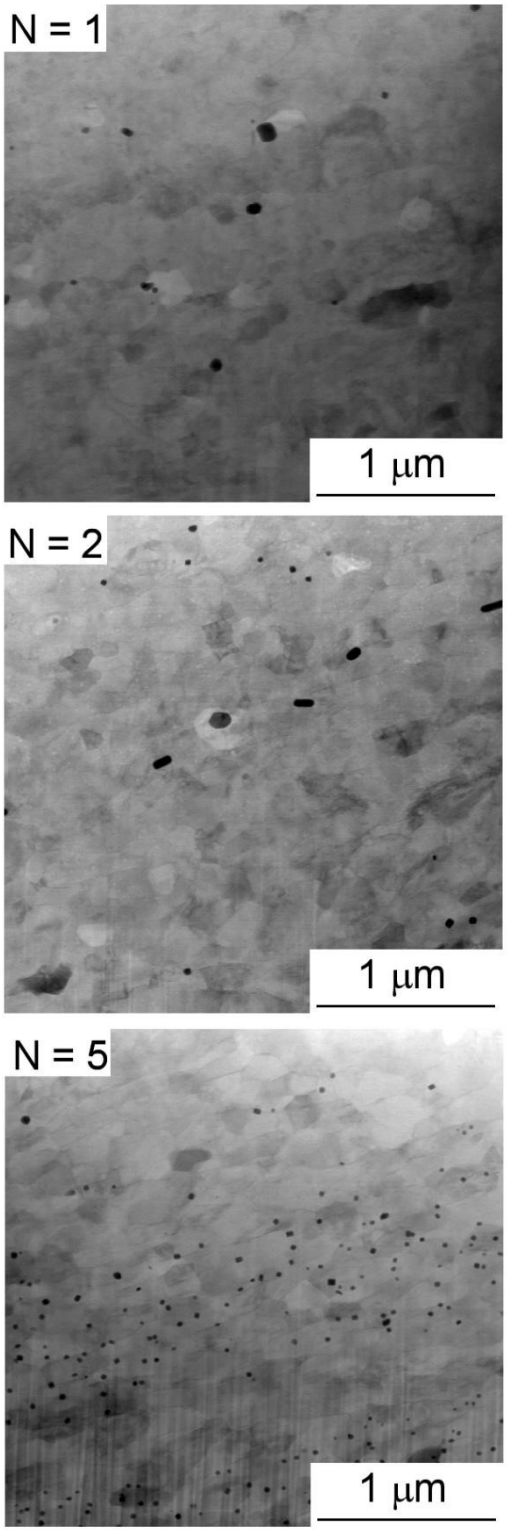

Figure 4.3 - BF-STEM images of samples processed by 1, 2 and 5 turns of HPT.

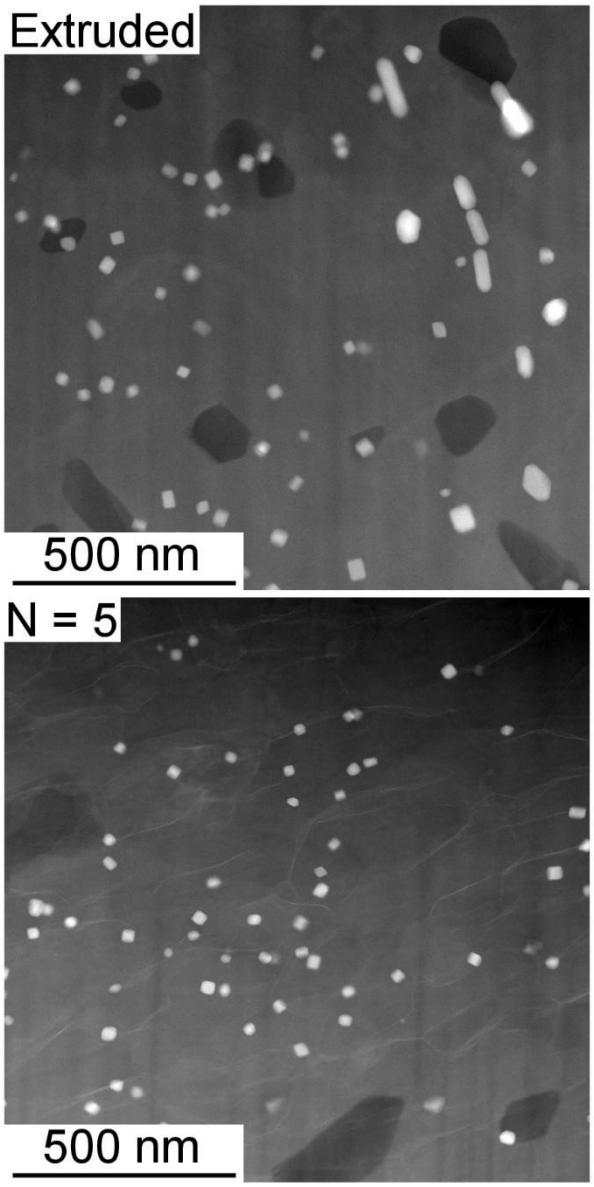

Figure 4.4 - HAADF images of the as-extruded sample and the material processed by 5 turns of HPT.

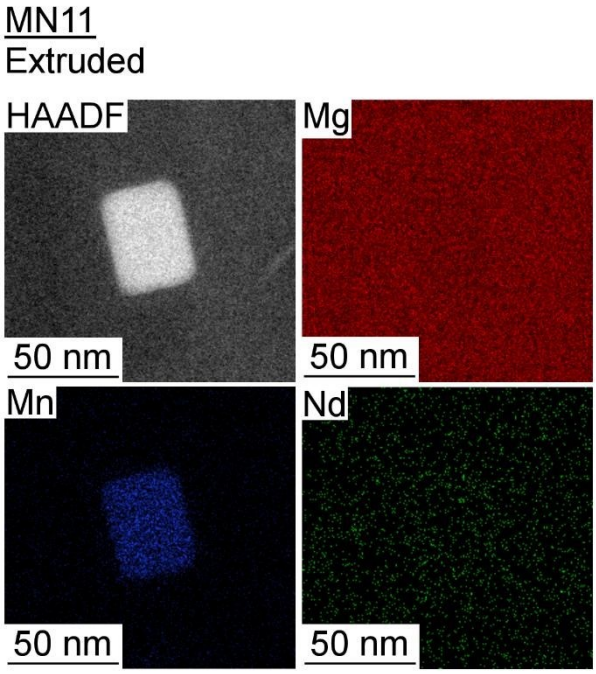

Figure 4.5 - HAADF image and the corresponding EDS elemental maps of a Mn particle in the as-extruded material.

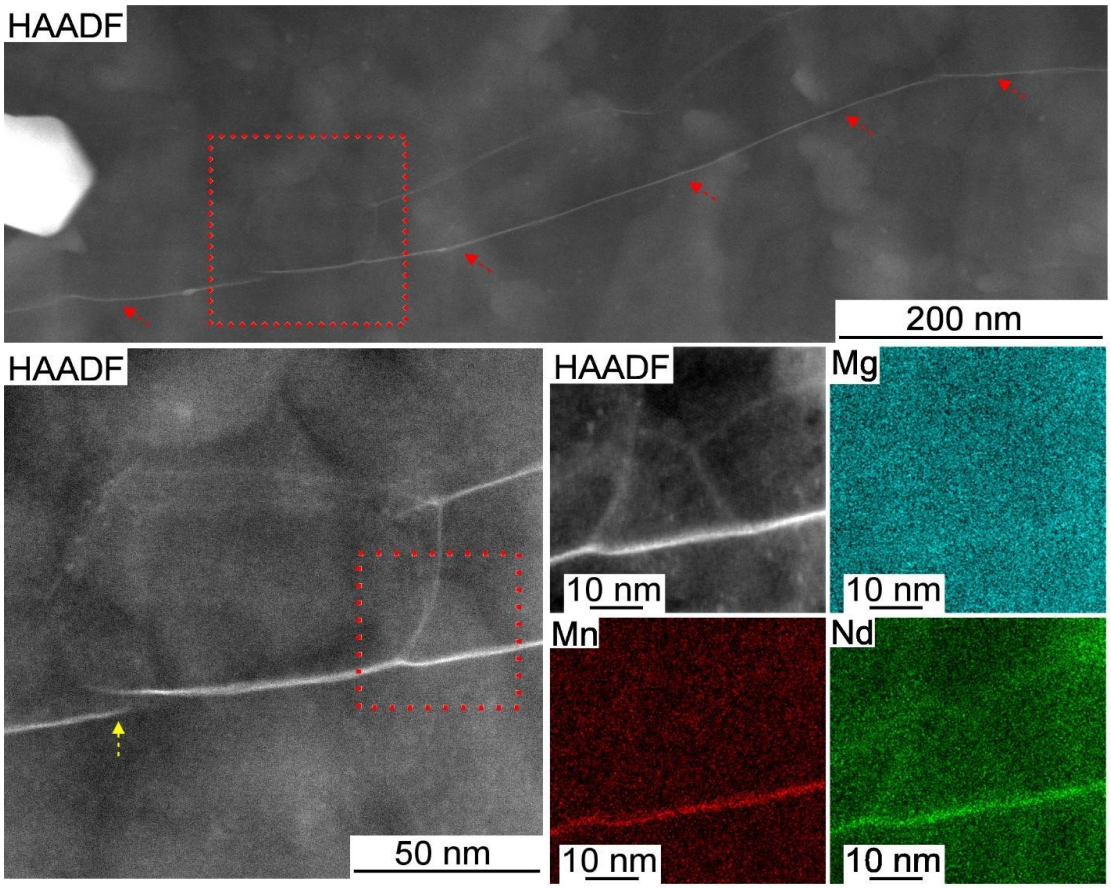

Figure 4.6 - HAADF images and EDS elemental maps of the sample processed to 1 turn of HPT.

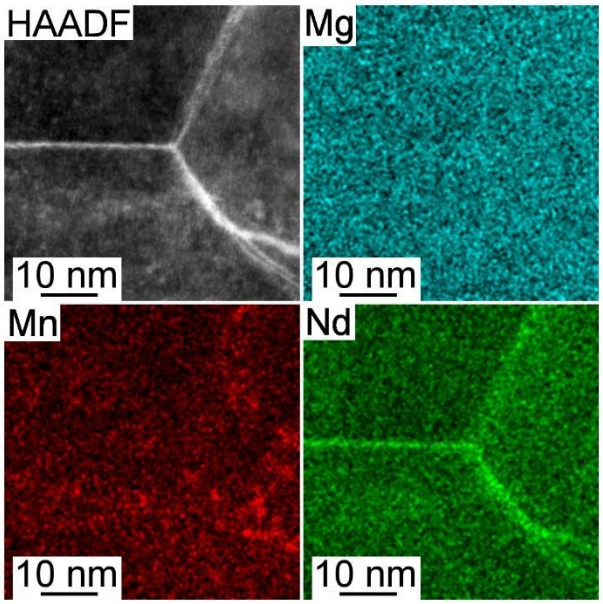

Figure 4.7 - HAADF image and EDS elemental maps of the sample processed to 2 turns of HPT.

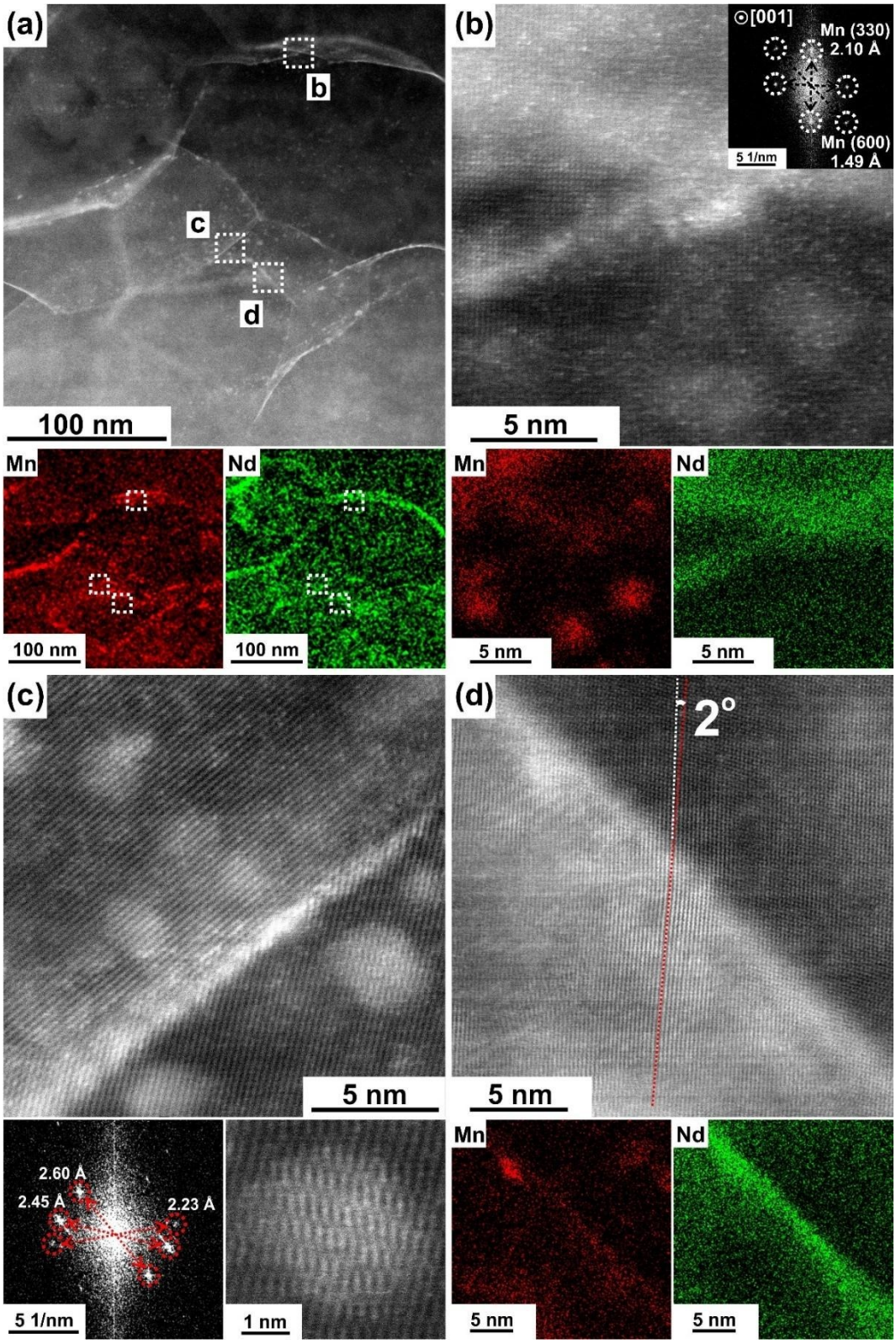

Figure 4.8 - (a) HAADF image and EDS elemental maps of the sample processed to 5 turns of HPT and (b-d) higher magnification images of selected areas.

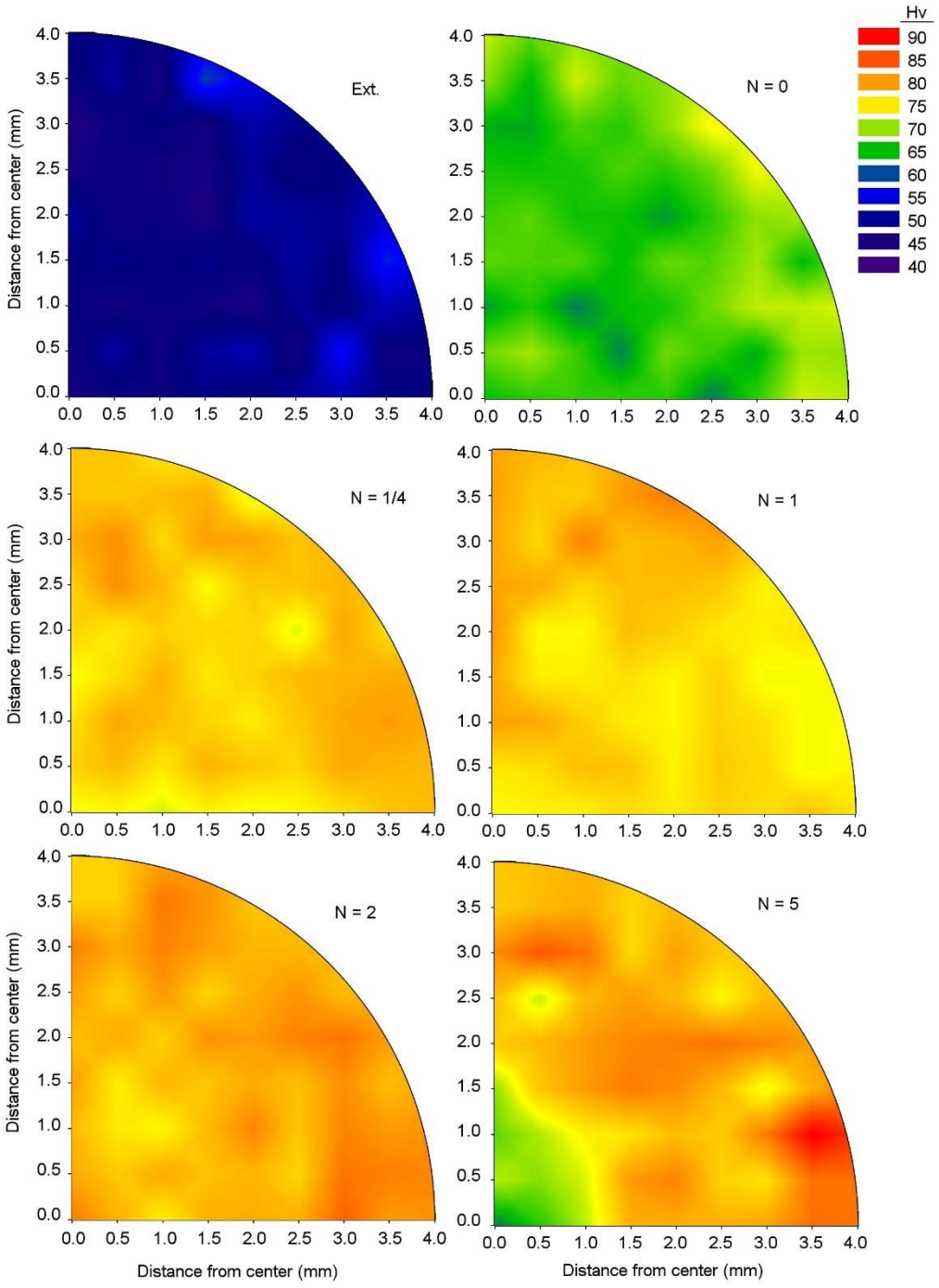

Figure 4.9 - Color-coded microhardness maps of samples in the as-extruded condition and after processing by HPT to 0, 1/4, 1, 2 and 5 turns.

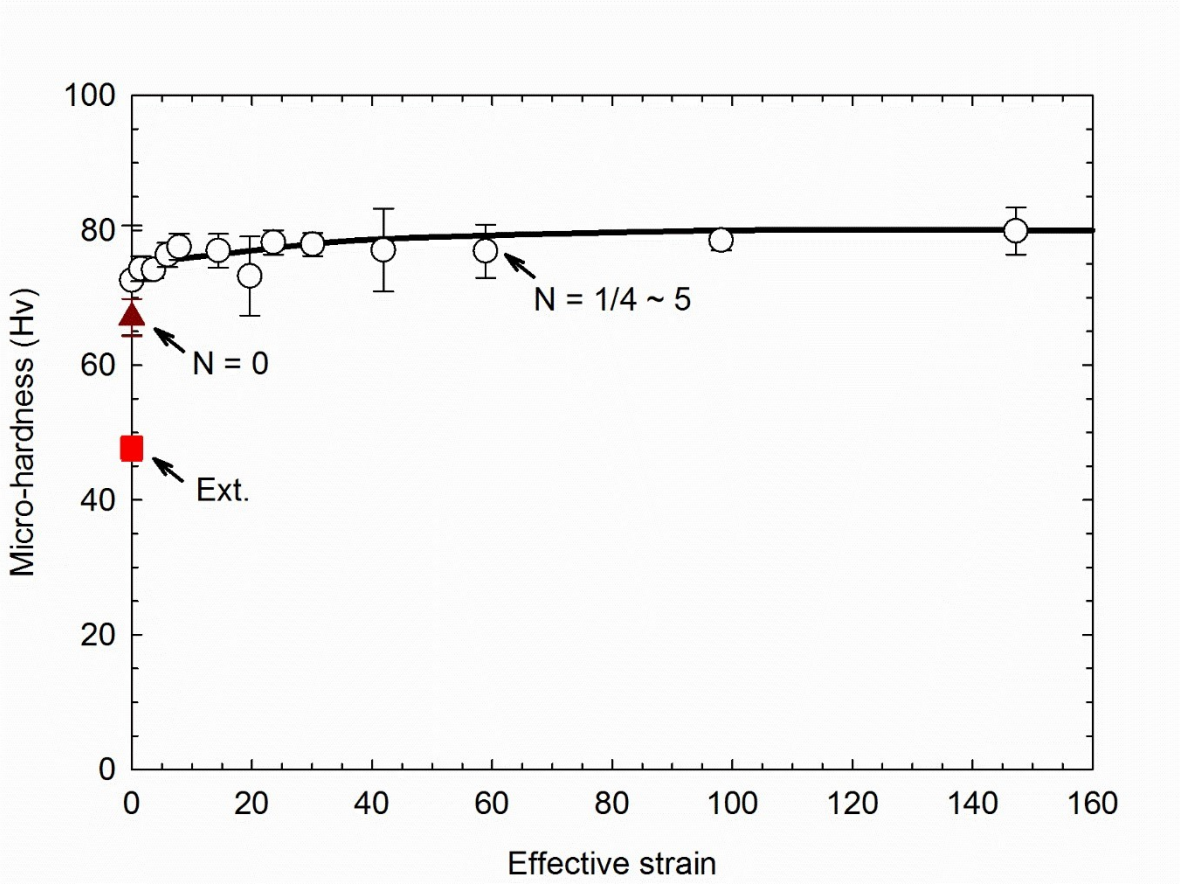

Figure 4.10 - Average microhardness values plotted as a function of the strain imposed during HPT processing.

References

[1] X. Sauvage, F. Wetscher, P. Pareige, Mechanical alloying of Cu and Fe induced by severe plastic deformation of a Cu–Fe composite, Acta Materialia 53(7) (2005) 2127-2135.

[2] A. Bachmaier, M. Kerber, D. Setman, R. Pippan, The formation of supersaturated solid solutions in Fe–Cu alloys deformed by high-pressure torsion, Acta Materialia 60(3) (2012) 860-871.

[3] X. Sauvage, N. Enikeev, R. Valiev, Y. Nasedkina, M. Murashkin, Atomic-scale analysis of the segregation and precipitation mechanisms in a severely deformed Al–Mg alloy, Acta Materialia 72 (2014) 125-136.

[4] Y. Zhang, S. Jin, P.W. Trimby, X. Liao, M.Y. Murashkin, R.Z. Valiev, J. Liu, J.M. Cairney, S.P. Ringer, G. Sha, Dynamic precipitation, segregation and strengthening of an Al-Zn-Mg-Cu alloy (AA7075) processed by high-pressure torsion, Acta Materialia 162 (2019) 19-32.

[5] A. Bachmaier, R. Pippan, High-Pressure Torsion Deformation Induced Phase Transformations and Formations: New Material Combinations and Advanced Properties, Materials Transactions 60(7) (2019) 1256-1269.

[6] M. Pouryazdan, B.J.P. Kaus, A. Rack, A. Ershov, H. Hahn, Mixing instabilities during shearing of metals, Nature Communications 8(1) (2017) 1611.

[7] J. Horky, A. Ghaffar, K. Werbach, B. Mingler, S. Pogatscher, R. Schaublin, D. Setman, P.J. Uggowitzer, J.F. Loffler, M.J. Zehetbauer, Exceptional strengthening of biodegradable MgZn-Ca alloys through high pressure torsion and subsequent heat treatment, Materials 12(15) (2019).

[8] D.A. Basha, R. Sahara, H. Somekawa, A. Singh, K. Tsuchiya, Effect of processing strain rate and temperature on interfacial segregation of zinc in a magnesium alloy, Materials Science and Engineering: A 703 (2017) 54-67.

[9] D.A. Basha, R. Sahara, H. Somekawa, J.M. Rosalie, A. Singh, K. Tsuchiya, Interfacial segregation induced by severe plastic deformation in a Mg-Zn-Y alloy, Scripta Materialia 124 (2016) 169-173.

[10] D.A. Basha, R. Sahara, H. Somekawa, J.M. Rosalie, A. Singh, K. Tsuchiya, Interfacial segregation induced by severe plastic deformation in a Mg–Zn–Y alloy, Scripta Materialia 124 (2016) 169-173.

[11] W.T. Sun, X.G. Qiao, M.Y. Zheng, X.J. Zhao, H.W. Chen, N. Gao, M.J. Starink, Achieving ultra-high hardness of nanostructured Mg-8.2Gd-3.2Y-1.0Zn-0.4Zr alloy produced by a combination of high pressure torsion and ageing treatment, Scripta Materialia 155 (2018) 2125.

[12] W.T. Sun, X.G. Qiao, M.Y. Zheng, C. Xu, S. Kamado, X.J. Zhao, H.W. Chen, N. Gao, M.J. Starink, Altered ageing behaviour of a nanostructured Mg-8.2Gd-3.8Y-1.0Zn-0.4Zr alloy processed by high pressure torsion, Acta Materialia 151 (2018) 260-270.

[13] J. Bohlen, S. Yi, D. Letzig, K.U. Kainer, Effect of rare earth elements on the microstructure and texture development in magnesium–manganese alloys during extrusion, Materials Science and Engineering: A 527(26) (2010) 7092-7098.

[14] N.V. Dudamell, P. Hidalgo-Manrique, A. Chakkedath, Z. Chen, C.J. Boehlert, F. Gálvez, S. Yi, J. Bohlen, D. Letzig, M.T. Pérez-Prado, Influence of strain rate on the twin and slip activity of a magnesium alloy containing neodymium, Materials Science and Engineering: A 583 (2013) 220-231.

[15] V. Herrera-Solaz, P. Hidalgo-Manrique, M.T. Pérez-Prado, D. Letzig, J. Llorca, J. Segurado, Effect of rare earth additions on the critical resolved shear stresses of magnesium alloys, Materials Letters 128 (2014) 199-203.

[16] C.Y. Wang, C.M. Cepeda-Jiménez, M.T. Pérez-Prado, Dislocation-particle interactions in magnesium alloys, Acta Materialia 194 (2020) 190-206.

[17] C.M. Cepeda-Jiménez, M. Castillo-Rodríguez, M.T. Pérez-Prado, Origin of the low precipitation hardening in magnesium alloys, Acta Materialia 165 (2019) 164-176.

[18] S. Tighiouaret, R. Lachhab, A. Hanna, H. Azzeddine, Y. Huang, T. Baudin, A.-L. Helbert, F. Brisset, D. Bradai, T.G. Langdon, Thermal Stability of an Mg–Nd Alloy Processed by High-Pressure Torsion, Advanced Engineering Materials 21(12) (2019) 1900801.

[19] K. Gusieva, C.H.J. Davies, J.R. Scully, N. Birbilis, Corrosion of magnesium alloys: the role of alloying, International Materials Reviews 60(3) (2015) 169-194.

[20] K. Saito, K. Hiraga, The Structures of Precipitates in an Mg-0.5 at%Nd AgeHardened Alloy Studied by HAADF-STEM Technique, Materials Transactions 52(10) (2011) 1860-1867.

[21] A.R. Natarajan, E.L.S. Solomon, B. Puchala, E.A. Marquis, A. Van der Ven, On the early stages of precipitation in dilute Mg–Nd alloys, Acta Materialia 108 (2016) 367-379.

[22] T.J. Pike, B. Noble, The formation and structure of precipitates in a dilute magnesium-neodymium alloy, Journal of the Less Common Metals 30(1) (1973) 63-74.

[23] W. Lefebvre, V. Kopp, C. Pareige, Nano-precipitates made of atomic pillars revealed by single atom detection in a Mg-Nd alloy, Applied Physics Letters 100(14) (2012) 141906.

[24] J.-F. Nie, Precipitation and Hardening in Magnesium Alloys, Metallurgical and Materials Transactions A 43(11) (2012) 3891-3939.

[25] Y.I. Bourezg, H. Azzeddine, T. Baudin, A.-L. Helbert, Y. Huang, D. Bradai, T.G. Langdon, Texture and microhardness of Mg-Rare Earth (Nd and Ce) alloys processed by highpressure torsion, Materials Science and Engineering: A 724 (2018) 477-485.

[26] Y.I. Bourezg, H. Azzeddine, L. Hennet, D. Thiaudière, Y. Huang, D. Bradai, T.G. Langdon, The sequence and kinetics of pre-precipitation in Mg-Nd alloys after HPT processing: A synchrotron and DSC study, Journal of Alloys and Compounds 719 (2017) 236-241.

[27] X. Zhou, X.-x. Yu, T. Kaub, R.L. Martens, G.B. Thompson, Grain Boundary Specific Segregation in Nanocrystalline Fe(Cr), Scientific Reports 6(1) (2016) 34642.

[28] R.Z. Valiev, Y.V. Ivanisenko, E.F. Rauch, B. Baudelet, Structure and deformaton behaviour of Armco iron subjected to severe plastic deformation, Acta Materialia 44(12) (1996) 4705-4712.

[29] J.J. Jonas, C. Ghosh, L.S. Toth, The equivalent strain in high pressure torsion, Materials Science and Engineering: A 607 (2014) 530-535.

[30] X. Sauvage, A. Duchaussoy, G. Zaher, Strain induced segregations in severely deformed materials, Materials Transactions 60(7) (2019) 1151-1158.

[31] K.S. Kormout, R. Pippan, A. Bachmaier, Deformation-Induced Supersaturation in Immiscible Material Systems during High-Pressure Torsion Advanced Engineering Materials 19(4) (2017) 1600675.

[32] R.B. Figueiredo, T.G. Langdon, Processing Magnesium and Its Alloys by HighPressure Torsion: An Overview, Advanced Engineering Materials 21(1) (2019) 1801039.

[33] C.L.P. Silva, R.B. Soares, P.H.R. Pereira, R.B. Figueiredo, V.F.C. Lins, T.G. Langdon, The Effect of High-Pressure Torsion on Microstructure, Hardness and Corrosion Behavior for Pure Magnesium and Different Magnesium Alloys, Advanced Engineering Materials 21(3) (2019) 1801081.

[34] K. Edalati, A. Yamamoto, Z. Horita, T. Ishihara, High-pressure torsion of pure magnesium: Evolution of mechanical properties, microstructures and hydrogen storage capacity with equivalent strain, Scripta Materialia 64(9) (2011) 880-883.

[35] H. Somekawa, D.A. Basha, A. Singh, Room temperature grain boundary sliding behavior of fine-grained Mg-Mn alloys, Materials Science and Engineering: A 730 (2018) 355362.

[36] H. Somekawa, A. Kinoshita, A. Kato, Great room temperature stretch formability of fine-grained Mg-Mn alloy, Materials Science and Engineering: A 697 (2017) 217-223.

5 FINAL CONSIDERATIONS

In the present work, the microstructural and mechanical evolution of the alloy Mg-1wt%Mn-1wt%Nd processed by HPT was evaluated for different levels of deformation to better understand the strengthening mechanisms of this alloy during severe plastic deformation. This evolution was observed using SEM, HAADF-STEM, and EDS mapping techniques.

HPT has considerably refined the (sub)grains even after processing through only one turn, quickly reaching saturation. Microstructural analysis by SEM / EDS also made it possible to observe the Mg-Nd intermetallics present in the alloy.

Using the HAADF-STEM technique alongside with EDS mapping, it was possible to verify the segregation of Nd and Mn atoms to grain boundaries. However, while Nd appears to segregate to the entire boundary network even at low levels of deformation, Mn segregation occurs more slowly and only to certain grain boundaries. In addition to segregation, Mn precipitates are fragmented during the HPT process, forming nanoclusters that are homogeneously distributed within the grains.

The alloy hardness increases considerably from ~ 40 HV in the as extruded material to a maximum of ~ 80 HV, reaching saturation with only 1 HPT turn. This increase in hardness is attributed to grain refinement and Nd segregation, as these phenomena also saturated with 1 HPT turn. It is concluded that Mn does not have a great influence on hardness, since the distribution of this element significantly changes with more turns of HPT through the fragmentation and formation of nanoclusters and further segregation.

The atomic-level characterization performed in this work allows a better understanding of the strengthening mechanisms of Mg alloys processed by HPT, essential for an efficient development of stronger alloys. That way, the resistance of the automotive and aerospace industries to the use of Mg gradually decreases, which would positively impact the environment by reducing the emission of polluting gases.

CONSIDERAÇÕES FINAIS

No presente trabalho, foi avaliada a evolução microestrutural e mecânica da liga Mg-1%Mn-1%Nd em peso processada por *HPT* para diferentes níveis de deformação com o objetivo de compreender melhor os mecanismos de endurecimento dessa liga durante uma deformação plástica severa. Essa evolução foi observada por meio das técnicas de *SEM*, *HAADF-STEM*, e mapeamento por *EDS*.

O *HPT* refinou consideravelmente os (sub)grãos, mesmo após o processamento em apenas um volta, atingindo rapidamente a saturação. A análise microestrutural por *SEM*/*EDS* também possibilitou observar os intermetálicos Mg-Nd presentes na liga.

Usando a técnica *HAADF-STEM* juntamente com mapeamento por *EDS*, foi possível constatar a segregação de átomos de Nd e de Mn para os contornos de grão. Entretanto, enquanto o Nd parece segregar para toda a rede de contornos mesmo em baixos níveis de deformação, a segregação do Mn ocorre de maneira mais lenta e apenas para certos contornos de grão. Além da segregação, os precipitados de Mn são fragmentados durante o processo de *HPT*, formando nano-aglomerados que se distribuem homogeneamente dentro dos grãos.

A dureza da liga aumenta consideravelmente de ~40 HV no material como extrudado até um máximo de ~80 HV, alcançando a saturação com apenas 1 volta de HPT. Esse aumento da dureza é atribuido ao refino de grão e à segregação de Nd, pois esses fenômenos também saturam com 1 volta de HPT. Conclui-se que o Mn não exerce grande influência na dureza, já que a distribuição desse elemento se altera com mais voltas de HPT, por meio da fragmentação e formação de nano-aglomerados e de mais segregação.

A caracterização a nível atômico realizada neste trabalho permite um maior entendimento dos mecanismos de endurecimento de ligas de Mg processadas por HPT, essencial para um desenvolvimento eficiente de ligas mais resistentes. Dessa maneira, a resistência das indústrias automotiva e aeroespacial ao uso do Mg vai diminuindo, o que impactaria positivamente o meio ambiente por meio da redução da emissão de gases poluentes.